AD-A179 616 DEMONSTRATION OF THE FEASIBILITY OF THE TUNING AND STIMULATION OF NUCLEAR RADIATION(U) TEXAS UNIV AT DALLAS RICHARDSON CENTER FOR QUANTUM ELECTRONIC.. 1/1

UNCLASSIFIED C B COLLINS 31 JAN 87 N00014-81-K-0653 F/G 20/5 NL

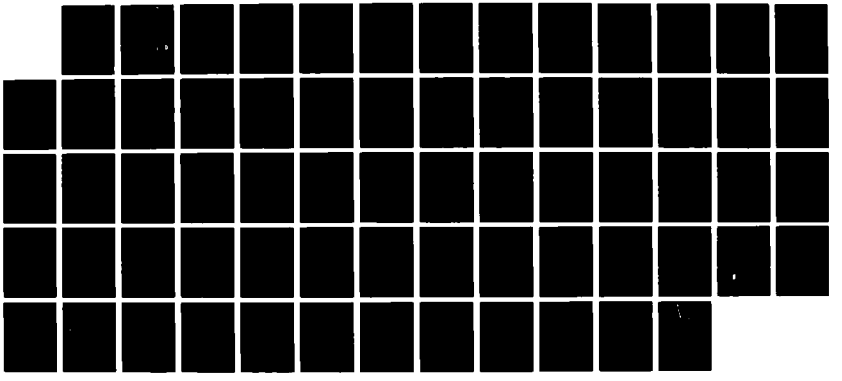

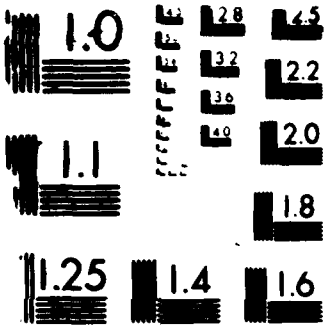

(12)

SECURITY CLASSIFICATION OF THIS PAGE (When Data Entered)

REPORT DOCUMENTATION PAGE

READ INSTRUCTIONS BEFORE COMPLETING FORM

1. REPORT NUMBER: XXUV86	2. GOVT ACCESSION NO.
3. RECIPIENT'S CATALOG NUMBER	
4. TITLE (and Subtitle): Demonstration of the Feasibility of the Tuning and Stimulation of Nuclear Radiation	5. TYPE OF REPORT & PERIOD COVERED: Annual Summary Report 1/1/86 - 12/31/86
6. PERFORMING ORG. REPORT NUMBER	
7. AUTHOR(s): Carl B. Collins	8. CONTRACT OR GRANT NUMBER(s): N00014-81-K-0653
9. PERFORMING ORGANIZATION NAME AND ADDRESS: University of Texas at Dallas, P.O. Box 830688, Richardson, TX 75083-0688	10. PROGRAM ELEMENT, PROJECT, TASK AREA & WORK UNIT NUMBERS: NR 395-072 410
11. CONTROLLING OFFICE NAME AND ADDRESS: Office of Naval Research, Physics Division, Arlington, VA 22217	12. REPORT DATE: January 31, 1987
	13. NUMBER OF PAGES: 48
14. MONITORING AGENCY NAME & ADDRESS(if different from Controlling Office)	15. SECURITY CLASS. (of this report): Unclassified
	15a. DECLASSIFICATION/DOWNGRADING SCHEDULE

16. DISTRIBUTION STATEMENT (of this Report)

Approved for public release; distribution unlimited.

17. DISTRIBUTION STATEMENT (of the abstract entered in Block 20, if different from Report)

18. SUPPLEMENTARY NOTES

19. KEY WORDS (Continue on reverse side if necessary and identify by block number)

Extreme Ultraviolet
Tunable XUV
Gamma Ray Laser

20. ABSTRACT (Continue on reverse side if necessary and identify by block number)

This project concerns the demonstration of the feasibility of the tuning and perhaps even stimulation of nuclear radiation. Theory has indicated that anti-Stokes Raman upconversion of intense but conventional long wavelength sources of radiation produced by scattering from isomeric states of nuclear excitation could lead to significant sources of tunable γ-radiation characterized by the natural Mossbauer widths of the lines. This would result in lines with sub-Angstrom wavelengths and (continued next page)

DD FORM 1 JAN 73 1473 EDITION OF 1 NOV 65 IS OBSOLETE
S/N 0102-LF-014-6601

SECURITY CLASSIFICATION OF THIS PAGE (When Data Entered)

20. ABSTRACT (continued)

widths of a few MHz. Whether or not these processes can reach threshold depends upon the resolution of basic issues lying in an interdisciplinary region between quantum electronics and nuclear physics that have not been previously addressed. It was the purpose of this work to study these issues experimentally.

ANNUAL SUMMARY REPORT

for the period

1 January 1986 through 31 December 1986

for

Office of Naval Research
Contract N00014-81-K-0653
Task No. NR 395-072

THE DEMONSTRATION OF THE FEASIBILITY OF THE TUNING AND STIMULATION OF NUCLEAR RADIATION

Short Title: GAMMA-RAY LASER

Principal Investigator: Carl B. Collins

The University of Texas at Dallas
Center for Quantum Electronics
P.O. Box 830688, Richardson, TX 75083-0688

87 4

TABLE OF CONTENTS

PROJECT DESCRIPTION

This project concerns the demonstration of the feasibility of the tuning and stimulation of nuclear radiation. It represents a critical line of investigation in our overall program concerned with the feasibility of a gamma-ray laser.

Theory, supported by our experiments conducted under this contract, has indicated that anti-Stokes Raman upconversion of intense but conventional laser radiation produced by scattering from isomeric states of nuclear excitation could lead to significant sources of tunable gamma radiation characterized by the natural Mossbauer widths of the lines. Further computations have suggested that this type of coherent, as well as a type of incoherent, optical pumping could even lead to appreciable levels of inversion of the populations of nuclear levels, thus supporting the growth of stimulated gamma-ray intensities. Whether or not these processes can reach threshold depends upon the resolution of basic issues that have not been previously addressed in an interdisciplinary region between quantum electronics and nuclear physics. It is the purpose of this contract work to study these issues experimentally in order to guide the development of the technology and methods needed to exploit the enormous potential of this effect.

SCIENTIFIC PROBLEM

The viability of the concept for the tuning of gamma radiation by adding the variable energy of an optical photon produced by a tunable laser depends upon the existence in the

nucleus of a particular arrangement of excited states. A suitable energy difference would would make it possible to dress the nuclear states with the laser photons. Transitions between the dressed states would then occur at the sum and difference frequencies characteristic of the nuclear transition, plus or minus the energies of integral numbers of laser photons.

Whether the necessary arrangements of nuclear states do exist is the central issue being addressed in this contracted work. Surprisingly, such information is currently unknown because such potentially useful states would lie in the "blind spots" of the conventional techniques of nuclear spectroscopy. Normal Mossbauer spectroscopy provides enormous resolution, but a tuning range that is inadequate by orders of magnitude to support any possible study of transitions to the intermediate states of a multiphoton process. Conversely, crystal spectrometers provide broad tuning ranges, but levels of resolution that miss by two orders of magnitude the threshold that would be necessary to separate the transitions to the initial and intermediate states. As a consequence, the ideal arrangement of nuclear energy levels needed for the Raman upconversion process could be a common occurrence that has gone unnoticed because of the inadequacies of conventional nuclear spectroscopy.

The critical problem in this research has two facets: 1) the development of an appropriate spectroscopic technique, and 2) the search for a suitable medium for a large-scale effect. The dressing of the nuclear states not only affects their energies, but also changes their transition properties. Forbidden nuclear transitions should become allowed so that the metastability of

isomeric states would be "switched off" as the states were dressed. This would greatly enhance the prospects for stimulating the gamma-ray transition, in addition to rendering it tunable. It is the development of the investigative instrumentation and the verification of these predicted effects that comprise the scientific problem addressed by this contract research.

TECHNICAL APPROACH

For the resolution of the central issue of the existence of potentially useful intermediate states in a multiphoton upconversion of optical photons to gamma-ray energies, it was first intended to demonstrate sum frequency generation in one case in which nonresonant intermediate states were known to exist. This was the case in which both initial and intermediate states were magnetic sublevels of the same nucleonic state and in which the transitions were mediated by the M1, magnetic dipole operator. Experimental data reproduced in the literature suggested that such a process had already been unknowingly demonstrated for the generation of radiofrequency sidebands to Mossbauer transitions at the sum and difference frequencies. This suggested the development of a new instrument, a Frequency Modulation Spectrometer for gamma-ray energies, designed to support the needed studies of nuclear structure with the precision of Mossbauer spectroscopy applied over a tuning range of energies lying considerably beyond the state-of-the-art at the time our work began. Pursuant to this goal, we are conducting a conventional single-photon Mossbauer experiment in the presence of an intense radiofrequency

field with measurement and parameterization of the conversion efficiency into the sum frequency line to determine the practical limits on the ultimate linewidths and tuning ranges that can be achieved. This technique will then be used in a "bootstrap" approach to support a search for accidentally resonant intermediate states. By replacing the radiofrequency excitation with tunable higher frequencies, it is expected that the tuning range of Mossbauer spectroscopy can be extended by further orders-of-magnitude.

PROGRESS DURING THIS REPORTING PERIOD

Instrumentation of FMS

The sum and difference frequency sidebands produced on intrinsic Mossbauer transitions has made possible very effective new instrumentation for high resolution spectroscopy at gamma-ray energies. A prototype version of this Frequency Modulation Spectrometer (FMS) was first described[1] by our laboratory in 1985, and subsequent refinements were made during the current reporting period under this contract and under a related SDI contract directed by ONR. This device monitors changes in the intensity of transmitted single-frequency gamma photons as a function of frequency of the long wavelength photons of the alternating magnetic field in which the absorbing nuclei are immersed.

During the past year our prototype "Nuclear Raman Spectrometer" was refined into more mature technology resulting in the Frequency Modulation Spectrometer (FMS) for gamma-ray energies (Figure 1). The original prototype device had required

a tedious level of manual interaction, and this was replaced with a fully-automated and computerized control system during the current reporting period. At its heart is a multi-channel scalar (MCS) and IEEE-488 GPIB interface with an Apple II+ computer. The MCS was designed to have a 100% duty cycle. The GPIB enables the spectrometer to sweep continuously through the frequencies of an rf magnetic field produced with a Wavetek frequency synthesizer. The Mossbauer drive allows the frequency of the gamma photon to be biased by a constant Doppler shift, if desired. In its present form, the FMS device has an instrumental resolution of 100Hz and a continuous tuning range of 10^9Hz with a stability of 0.1Hz/sec with no mechanical movements required anywhere. These characteristics are comparable to a Mossbauer spectrometer with a means of shifting the gamma-ray source, having a resolution of 10nm/sec and a range of 100mm/sec with a stability of 0.01nm/sec/sec. Demonstration spectra were acquired with ^{57}Fe showing isomer shifts and thermal shifts. Because we were using a modulation type of spectroscopy, the static features could be suppressed, and these different effects were obtained with unprecedented clarity.

In operation, FMS of ^{57}Fe provides a direct measurement of rf sideband positions and intensities from which one can extrapolate information about the transitions between Zeeman split energy levels (parent transitions), labeled 1 through 6 in Figure 2. Radiofrequency sidebands have been labeled as a parent transition preceded by a number of +'s or -'s, the number of which corresponds to the number of rf field energy quanta

(order of the sideband) added to or subtracted from the parent transition. The symmetrically opposed parent transitions 1 and 6 are separated by 123.7 MHz in pure iron. Applying a 61.85 MHz alternating magnetic field to the Fe foil produces (+1) and (-6) sidebands which overlap in the symmetric center, or transition center, of the hyperfine structure of the ^{57}Fe. The energies of the gamma ray emitted by the source and the transition center of the absorber differ by the isomer shift, Δ (Figure 3a). In FMS the Stokes sideband from parent transition 6, (-6) would be detected at a frequency of (61.85-Δ) MHz while the anti-Stokes sideband from parent transition 1, (+1) would be detected at a frequency of (61.85+Δ) MHz (Figure 3b and c). Therefore, FMS should produce a spectrum with two peaks around 60 MHz, separated by 2Δ.

If we apply a small Doppler shift, ∂, to the source, we should obtain an FMS spectrum with two peaks around 60 MHz, separated by 2(Δ + ∂) (Figure 4). Classically, the frequencies at which sidebands appear, fs, is simply

$$fs(MHz) = [\ v - (P_j + iso)] * (11.6/ord), \qquad (1)$$

where P_j is the position of the j'th parent transition (mm/sec), v is the velocity of the source (mm/sec), iso is the isomer shift (mm/sec), and ord is the order of the sideband of interest. The source used was in a Pd lattice (iso = -0.185).

Radiofrequency sideband positions are also apparently affected by the intensity of the rf magnetic field (Figure 5). It is yet to be determined whether sideband position is a function of intensity as well as frequency of the rf magnetic

field, or whether the temperature shift of the parent transitions is being detected, or both. Since we start with a negative isomer shift, raising the temperature of the absorber should reduce the energy difference between the source transition and the transition center of the absorber. Therefore, increasing the rf field intensity should raise the temperature of the absorber and in turn decrease the isomer shift.

It seems clear that, in addition to providing information about sideband intensity and position, FMS could also prove to be a means for direct and accurate measurement of isomer and temperature shifts, spectroscopic quantities that are difficult to measure with Mossbauer spectroscopy as usually practiced because of the difficulty in obtaining such small velocities with such precise control. For the purposes of the gamma-ray laser program, it is the combination of narrow instrumental width and large tuning range that offers the greatest attractions.

To dress an isomeric state requires a certain arrangement of nuclear levels that would make them undetectable to conventional techniques of nuclear spectroscopy. Our method of FMS is the only means found to date that can be used to search for this combination among the 29 best candidates for a gamma-ray laser. The successes of the new FMS apparatus for nuclear spectroscopy indicate that a much higher resolution, by perhaps several more orders of magnitude, can be achieved through a reasonable upgrade of the apparatus. If the range of tunability does extend to the ferromagnetic spin resonance (FSR) frequency, then it will be possible to construct a swept frequency device

capable of continuously tuning over a range of 10^{11} linewidths, an enormous improvement in the state-of-the-art of nuclear spectroscopy.

Theory of FMS

Most laboratory sources of gamma radiation emit at levels of intensity corresponding to single photon conditions. Mossbauer experiments are rarely conducted at such great intensities that the detection of two photons would be probable in the transit time spent between source and absorber. Under those conditions, the perception of gamma rays as streams of particles is instinctive. Nevertheless, as elements of electromagnetic radiation they must also be considered as carrier waves of high frequency. As the name implies, the Frequency Modulation Spectrometer derives its operation from the modulation of the gamma-ray carrier and represents a translation into the nuclear domain of one of the powerful techniques of laser spectroscopy at the atomic level. As described above, the device itself works better than the theory describing it, and during the current reporting period emphasis developed upon refining and validating the dressed state theory describing the origin of the carrier modulation. Reviewed in the following material will be five different approaches to a comprehensive theoretical description. Not published elsewhere, each is being reported here as each approach is useful in defining acceptable levels of approximation.

CONTEXT OF THEORETICAL EFFORTS

In our version of FMS, the spectrum of the gamma photons emitted by the source is modulated by its passage through a thin, ferromagnetic foil immersed in a radiofrequency magnetic field[2]. Most work has been done upon ^{57}Fe with the radiofrequency magnetic field being applied in the plane of the foil. Although the interaction energy of the nuclear magnetic moment directly with the applied magnetic field is insufficient to cause a significant perturbation of the system, the applied magnetic field is sufficient to cause the direction of the magnetization within the material, $\vec{M}(t)$, to precess in a complicated manner and this interaction of the nuclear moment with $\vec{M}$ is of significant magnitude.

Ferromagnetism is a cooperative magnetic behavior resulting from the exchange interaction between the electrons. In ferromagnetic materials, the principal effect of the exchange interaction is to cause parallel ordering or alignment of the atomic spins in a common direction, so that there is a large spontaneous magnetization even in the absence of an applied field. Maximum ordering is obtained at $0^{\circ}K$ where the randomizing effect of thermal agitation disappears. At the Curie temperature T_C the magnetic ordering is destroyed by thermal agitation, and the spontaneous magnetization disappears. Between these two extremes a sample of ferromagnetic material is usually divided into small volumes called domains, which may vary in size, shape and direction of magnetization. Within each domain, the magnetization is uniform and has the maximum or saturation value, M_s.

characteristic of the material and the temperature. *Within a ferromagnetic material, the magnetization vector $\vec{M}(t)$ may vary in direction but not in magnitude, even when traversing a domain wall.* Therefore, changes of the magnetization are precessions and must be described by equations which reflect this.

The magnetic field at the site of the ^{57}Fe nucleus is the sum of several large terms which may be positive or negative. In an ^{57}Fe foil the magnetic field at the nucleus has been determined to be about 330×10^3 Oersteds in the direction opposite to the local direction of the bulk magnetization, $\vec{M}(t)$. The electrons respond to the changes of $\vec{M}(t)$ quite rapidly since the magnetic moments of the electrons are strongly coupled to $\vec{M}(t)$ (the cooperative effect). Thus, in response to any applied fields, the magnetic field at the site of the nucleus also precesses in a manner which reflects the precession of the bulk magnetization. For this reason, the motion of the magnetization $\vec{M}(t)$ must be determined as a function of time as a part of any comprehensive description of the ultimate effects of applied H fields upon nuclear states.

The equation of motion of the magnetization vector $\vec{M}(t)$ is determined by the Landau-Lifshitz equation:

$$-(1/|\gamma|)\, d\vec{M}(t)/dt = (\vec{M} \times \vec{F}) - \lambda\, [\vec{F} - (\vec{M}\cdot\vec{F})\, \vec{M}/M_s^2] \quad . \quad (2)$$

The gyromagnetic ratio of the electron is given by $-|\gamma|$, and λ is an experimental parameter obtained from ferromagnetic resonance studies, $\lambda/M_s \sim 10^{-3}$. The magnetic field $\vec{F}$ in equation (2) is the vector sum of four contributions: 1) the magnetic field required to simulate the magnetic anisotropy effects inherent to

the crystal structure of the material, 2) the "magnetostatic" fields due to the finite size of the sample, 3) the exchange field, which represents a potential energy term leading to the ordering of neighboring magnetic dipole moments on a microscopic scale, and 4) the applied magnetic field. The solutions[3,4] to equation (2) depend strongly on the anisotropy of the material and on the geometry of the sample and are usually of an exceedingly complicated nature. Approximations were developed to varying degrees as part of each of the different approaches to the nuclear sideband problem.

During the past year our efforts to develop a model of the modulation of the gamma spectrum have focused upon the following five approaches, to be summarized in this report below:

1. The refinement of the theoretical approach initiated by C. B. Collins and B. D. DePaola[2] in Optics Letters 10, 25 (1985) culminating in the results presented at the 1986 IQEC meeting. We have referred to this as the multiphoton processes in nuclear states.

2. A literature search and study of the applicability of the "dressed atom" approach of C. Cohen-Tannoudji.

3. The development of a coherent switch model of the magnetization $\vec{M}(t)$ by integrating the Landau-Lifshitz equation. This model was specific for a thin ferromagnetic foil. The solution for $\vec{M}(t)$ is in agreement with results presented elsewhere.[4]

4. The development of a domain wall passage model. This research does not appear to have been fruitful, although it may

still be of use.

5. In collaboration with Professor P. Berman of New York University, the development of solutions to the time dependent Schroedinger equation utilizing information about the magnetization derived from approach 3. The resulting method appears to be the best approach. The computer code is in the process of development and is being verified first for the static case.

1) Multiphoton Processes in Nuclear States of ^{57}Fe in a Ferromagnetic Foil Immersed in a Radiofrequency Magnetic Field

The time-dependent Schroedinger equation of the ^{57}Fe nucleus embedded in a ferromagnetic foil immersed in an rf magnetic field is

$$i\hbar(d\Psi/dt) = H_A\Psi - \{\vec{H}_{app}(t)\cdot\vec{\mu} + \vec{M}(t)\cdot\vec{\mu} + \vec{H}_d(t)\cdot\vec{\mu} + \vec{H}_{dn}(t)\cdot\vec{\mu}\}\Psi \quad (3)$$

where

Ψ = the eigenstate of the system,

H_A = the atomic Hamiltonian associated with quantum number(s) α,

$\vec{\mu}$ = the magnetic moment of the nucleus,

$\vec{H}_{app}$ = the applied radiofrequency magnetic field (a few gauss) with frequency ω_1,

$\vec{M}$ = the magnetization of the material (kilogauss),

$\vec{H}_d$ = the demagnetizing field due to the surface poles developed when $\vec{M}$ rotates out of the plane of the foil (kilogauss),

$\vec{H}_{dn}$ = the demagnetizing field due to the poles developed when the nuclear magnetic moment $\vec{\mu}$ rotates out of the plane of the foil (very small).

The expression in the brackets represents the interaction of the nuclear magnetic moment, $\vec{\mu}$, with the vector sum of all of the magnetic fields to which the nucleus is subjected. The interaction of the magnetic field with the electrons is included in the behavior of $\vec{M}$ and therefore does not require another term. This notation and approach are essentially the same as outlined by Collins and DePaola[2].

Since the terms $\vec{H}_{app}(t)\cdot\vec{\mu}$ and $\vec{H}_{dn}(t)\cdot\vec{\mu}$ are small when compared to the other terms in the Hamiltonian, they are neglected.

The simplified time dependent Schroedinger equation becomes

$$i\hbar\,(\partial\Psi/dt) = H_A\,\Psi - \{\vec{M}(t)\cdot\vec{\mu} + \vec{H}_d(t)\cdot\vec{\mu}\}\,\Psi \qquad (4)$$

in the fixed laboratory coordinates.

A new coordinate system is defined in the laboratory, such that the magnetization $\vec{M}$ in the plane of the foil corresponds to the z axis, that is, as $\vec{M}$ responds to the applied magnetic field (by rotating in the plane of the foil), the foil is rotated about an axis perpendicular to the foil in such a way that $\vec{M}$ <u>always</u> lies along the z axis of the laboratory coordinates. Doppler shifts are introduced because the foil is moving, but since the absorption spectrum is observed along an axis perpendicular to the foil, only the second order transverse Doppler shift occurs, which should be negligible. This coordinate system is denoted as primed in the following material. In it $\vec{M}$ has constant magnitude and direction (z axis) as shown in Figure 6. Equation (4) may be rewritten

$$i\hbar\,(\partial\Psi'/\partial t) = H_A\,\Psi' - \{\vec{M}\cdot\vec{\mu} + \vec{H}_d(t)\cdot\vec{\mu}\}\,\Psi' \quad . \qquad (5)$$

The magnetic moment of the nucleus, $\vec{\mu}$, is related to its angular

momentum through the equality

$$\vec{\mu} = (g_x \mu_N/\hbar)\,\vec{J} \qquad (6)$$

where x denotes either the ground (g) or excited (e) state of the nucleus. The symbol μ_N stands for the nuclear magneton.

$$\mu_N = (e\hbar/2M) = 0.505 \times 10^{-26} \text{ amp-m}^2 \quad , \qquad (7)$$

in the MKS system of units.

The Hamiltonian of a particularly useful basis set of eigenstates and energies is obtained from,

$$H_B = H_A - \vec{M}\cdot\vec{\mu} = H_A - \hbar\omega_x J_z \quad , \qquad (8)$$

where $\hbar\omega_x$ corresponds to the total splitting of the x level by the magnetization $\vec{M}$,

$$\hbar\omega_x = g_x \mu_N M_s \quad . \qquad (9)$$

In the basis set, the time dependent Schroedinger equation of the x state,

$$i\hbar\,(\partial\Psi_o'/\partial t) = H_A\,\Psi_o' - \hbar\omega_x J_z\,\Psi_o' \quad , \qquad (10)$$

has solutions of the form,

$$\Psi_o'(\alpha_x, J', m') = |\alpha_x, J', m'\rangle \exp[-i(E_{\alpha_x}/\hbar - m'\omega_x)t]. \qquad (11)$$

The quantum number(s) α_x describe the nuclear state x with energy E_{α_x}, in the absence of any magnetization field in the material or any applied field. The angular momentum state of the nucleus in the primed coordinate system is described by J' and m'. These basis states of the system might be described as the "non-interacting basis" states.

The interacting state Ψ' can be derived from the basis state Ψ_o' by means of a rotation through an angle θ_x about an axis parallel to $\vec{H}_d(t)$. This rotation operator is Hermitian and unitary and of the form

$$R = \exp[i\phi_x \hat{n}\cdot\vec{J}] = \exp(i\phi_x J_d) \quad . \tag{12}$$

where $\hat{n}$ is a unit vector parallel to the axis of rotation. The interacting state is given by

$$\Psi'_x = e^{(i\phi_x J_d)}\, \Psi'_o(\alpha_x, J', m') \quad . \tag{13}$$

Combining equations (5) and (13), the time dependence of the angle ϕ_x is given by the equation

$$(\partial\phi_x/\partial t) = g_x \mu_N H_d(t)/\hbar \quad . \tag{14}$$

If $H_d(t)$ is known, the angle $\phi_x(t)$ can be computed numerically and therefore may be considered a known function.

The transition amplitude is determined by

$$i\hbar(da_{eg}/dt) = i\hbar\, \dot{a}_{eg} = \tag{15}$$

$$\int\left[e^{(+i\phi_e J_d)}\, \Psi'_o(\alpha_e, J', m')\right]^* V_\gamma e^{-i\omega_\gamma t}\left[e^{(+i\phi_g J_d)}\, \Psi'_o(\alpha_g, J', m')\right] d\tau \, .$$

Since R is Hermitian and unitary, this equation may be rewritten

$$i\hbar\, \dot{a}_{eg} = \tag{16}$$

$$e^{-i\omega_\gamma t}\int\left[e^{[+i(\phi_e - \phi_g)J_d]}\, \Psi'_o(\alpha_e, J', m')\right]^* W_\gamma\, \Psi'_o(\alpha_g, J', m')\, d\tau$$

where

$$W_\gamma = e^{(-i\phi_g J_d)}\, V_\gamma\, e^{(+i\phi_g J_d)} \approx V_\gamma \quad . \tag{17}$$

The operator J_d is not diagonal in the primed coordinate system since $\hat{n}$ is perpendicular to $\vec{M}$ (the z axis). It is necessary to use the finite rotation matrix[10] to transform into a system in which the z axis is parallel to $\hat{n}$. After operating with J_d, then the finite rotation matrix is again used to return to the primed laboratory system.

The time derivative of the total transition amplitude in terms of $\langle\Psi'_e(m_e)|W_\gamma|\Psi'_g(m_g)\rangle$ is given by

$$
\begin{aligned}
i\hbar\,\dot{a}_{eg} = (1/2)^2 \; [& c_B \exp[i\Omega_1 t] \langle -3/2|W_\gamma|-1/2\rangle R_1(t) \\
& + c_B \exp[i\Omega_2 t] \langle -1/2|W_\gamma|-1/2\rangle R_2(t) \\
& + c_B \exp[i\Omega_3 t] \langle +1/2|W_\gamma|-1/2\rangle R_2(t) \\
& + c_A \exp[i\Omega_4 t] \langle -1/2|W_\gamma|+1/2\rangle R_2(t) \\
& + c_A \exp[i\Omega_5 t] \langle +1/2|W_\gamma|+1/2\rangle R_2(t) \\
& + c_A \exp[i\Omega_6 t] \langle +3/2|W_\gamma|+1/2\rangle R_1(t)]
\end{aligned}
\tag{18}
$$

where Ω_i is the detuning of the i^{th} transition as shown in Figure 7. That is,

$$\Omega_i = (\Delta E_i/\hbar) - \omega_\gamma \quad . \tag{19}$$

where ΔE_i is the energy of the i^{th} transition. The concentrations of the ground state levels are c_A and c_B for $m = -1/2$ and $m = +1/2$ respectively. If the angle ϕ is defined by

$$\phi \equiv \phi_e - \phi_g \quad . \tag{20}$$

the factors $R_1(t)$ and $R_2(t)$ which appear in the transition amplitudes are defined as follows:

$$R_1(t) = (1 + \sqrt{3})\, e^{-i(3\phi/2)} + (3 - \sqrt{3})\, e^{i\phi/2} \tag{21a}$$

$$R_2(t) = (3 + \sqrt{3})\, e^{-i(3\phi/2)} + (1 - \sqrt{3})\, e^{i\phi/2} \quad . \tag{21b}$$

The transitions probabilities are calculated from

$$\lim_{t\to\infty} \frac{1}{t}(-i\hbar\, a_{eg})(+i\hbar\, a^*_{eg}). \tag{22}$$

When $R_1(t)$ and $R_2(t)$ are expanded in Fourier series.

$$R_j(t) = \sum_{-\infty}^{+\infty} n\, (R_j)_n\, e^{(-in\omega_1 t)} \quad . \tag{23}$$

there are two components to the transition probability which survive the time averaging procedure. The first is the "normal" contribution given by

$$W_{eg} = \frac{2\pi}{\hbar^2}\left(\frac{1}{2}\right)^4 \sum_{-\infty}^{+\infty} n \Big\{ (R_1)_n (R_1)_n^* \Big[c_B^2 |\langle -3/2 | W_\gamma | -1/2 \rangle|^2 \, \delta(\Omega_1 - n\omega_1)$$

$$+ c_A^2 |\langle +3/2 | W_\gamma | +1/2 \rangle|^2 \, \delta(\Omega_6 - n\omega_1) \Big]$$

$$+ (R_2)_n (R_2)_n^* \Big[c_B^2 |\langle -1/2 | W_\gamma | -1/2 \rangle|^2 \, \delta(\Omega_2 - n\omega_1)$$

$$+ c_B^2 |\langle +1/2 | W_\gamma | -1/2 \rangle|^2 \, \delta(\Omega_3 - n\omega_1)$$

$$+ c_A^2 |\langle -1/2 | W_\gamma | +1/2 \rangle|^2 \, \delta(\Omega_4 - n\omega_1)$$

$$+ c_A^2 |\langle +1/2 | W_\gamma | +1/2 \rangle|^2 \, \delta(\Omega_5 - n\omega_1) \Big] \Big\} \quad . (24)$$

After $R_1(t)$ and $R_2(t)$ have been expanded in terms of their Fourier components, a typical term in the product of the two expansions shown in (22) is of the form

$$c_i (ME)_i \; c_j^* (ME)_j^* \sum_{m,n} (R_i)_n (R_j)_m^* \left[\frac{e^{i(\Omega_i - n\omega)t} - 1}{\Omega_i - n\omega} \right] \left[\frac{e^{-i(\Omega_j - m\omega)t} - 1}{\Omega_j - m\omega} \right] , (25)$$

where $(ME)_i$ is the matrix element of the i^{th} transition. When the time average is taken as shown in expression (22), this term is zero for all $m \neq n$. The summation over m collapses to one term which does not vanish when the time average is taken. When $m = n$, the equality[10] in the limit $t \to \infty$,

$$\lim_{t \to \infty} \frac{\sin^2 \alpha t}{\pi t \alpha^2} = \delta(\alpha) \qquad (26)$$

may be used, which introduces the delta functions of frequency.

In reality, the delta functions of frequency must be replaced by Lorentzian distributions centered at the position of the delta function. The width of the Lorentzian corresponds to the lifetime of the excited state. The parent lines of the transition, that is, the spectrum in the absence of the rf magne-

tic field, correspond to the n = 0 amplitudes,

$$W_{eg}^{0} = \frac{2\pi}{\hbar^2}\left(\frac{1}{2}\right)^4 \Big\{ |(R_1)_0|^2 \Big[c_B^2 |\langle -3/2|W_\gamma|-1/2\rangle|^2 \, \delta(\Omega_1) + c_A^2 |\langle +3/2|W_\gamma|+1/2\rangle|^2 \, \delta(\Omega_6) \Big] + |(R_2)_0|^2 \Big[c_B^2 |\langle -1/2|W_\gamma|-1/2\rangle|^2 \, \delta(\Omega_2) + c_B^2 |\langle +1/2|W_\gamma|-1/2\rangle|^2 \, \delta(\Omega_3) + c_A^2 |\langle -1/2|W_\gamma|+1/2\rangle|^2 \, \delta(\Omega_4) + c_A^2 |\langle +1/2|W_\gamma|+1/2\rangle|^2 \, \delta(\Omega_5) \Big] \Big\} . \quad (27)$$

The delta functions of frequency indicate that the parent lines will be observed at their normal frequencies,

$$\Omega_i = \text{detuning} = 0 \quad \text{or} \quad \Delta E_i/\hbar = \omega_\gamma . \quad (28)$$

The intensity of the first order sideband may be found in the same manner by taking either $n = \pm 1$. For $n = +1$, the frequencies of the first order sidebands in the absorption spectrum is found by taking

$$\Omega_i - \omega_1 = (\Delta E_i/\hbar) - \omega_\gamma - \omega_1 = 0 , \quad (29)$$

or

$$[(\Delta E_i/\hbar) - \omega_1] = \omega_\gamma . \quad (30)$$

Thus, $n = +1$ corresponds to the first negative sideband and conversely $n = -1$ corresponds to the first positive sideband. The absolute magnitudes of $(R_i)_n$ govern the amplitudes of the sidebands. For this reason, it is vitally important to have an adequate model of the behavior the magnetization $\vec{M}$ as a function of time.

The second component is a quantum enhancement which adds on to the "normal" curve whenever the condition,

$$\Omega_i - \Omega_j = p\omega_1 \quad (31)$$

(p is any positive or negative integer) is satisfied, that is,

whenever two transition energies differ by an integral number of photons in the rf field. The intensity given by the "normal" curve is increased by the amount

$$\frac{2\pi}{\hbar^2}\left(\frac{1}{2}\right)^4 \sum_n \left[K(R_i)_n (R_j)^*_{n-p} + K^*(R_i)^*_n (R_j)_{n-p}\right] \delta(\Omega_i - n\omega_1), \quad (32)$$

where,

$$K = c_i\, c_j^*\, (ME)_i\, (ME)_j^* \quad . \quad (33)$$

As can be seen from expression (33), the enhancements to the absorption spectrum fall on the same frequencies as the usual sidebands, including the parent, and occur only when equation (31) is satisfied. If i = 1 or 6, then $R_i \rightarrow H_1$. For all other values of the index i, then $R_i \rightarrow R_2$. The index j follows the same rules. For this reason, the quantum enhancement must be determined on a case-by-case basis.

At this point the model is a direct extension of the one originally proposed by DePaola and Collins[2] which was limited in validity to the vicinity of a moving domain wall where the angle of rotation of the magnetization $\vec{M}(t)$ in the plane of the foil is large. The extension realized in this section as characterized in equations (24) and (32) is more generally valid. Unfortunately both models share the dependence on the rather simplified description of the magnetization which strictly confines $\vec{M}(t)$ to a plane. Not surprisingly, neither one adequately describes the enhancement of the sideband intensity observed in ^{57}Fe near the applied frequency of 45 MHz. This enhancement of the sideband amplitude was thought to be due to the mixing of the Zeeman levels of the ground state by the

applied magnetic field. For a better understanding of the mixing effects of an intense field, the 'dressed state theory' of C. Cohen-Tannoudji[5,6,7] and S. Haroche[8,9] was studied, because it had been refined and experimentally verified to a very high degree of accuracy for analogous cases in atomic physics.

Also, before proceeding further, it is necessary to develop a better model for the behavior of the magnetization $\vec{M}(t)$ in the presence of an applied rf field. To accomplish this, it is necessary to integrate the Landau-Lifshitz equation (equation 2) as discussed in sections 3 and 4.

2) "Dressed State" Theory

At first, the work of C. Cohen-Tannoudji[5,6,7] and S. Haroche[8,9] on atoms immersed in a strong electromagnetic field of a single frequency (optical or radio frequency) is very attractive conceptually. It departs considerably from the usual approach in which the interaction of the atom with the applied electromagnetic field is considered as a perturbation to be handled using standard perturbation theory. The need for an alternative arises from the fact that perturbation theory is not appropriate when the strength of the interaction is large due to the presence of very strong fields. In the dressed state theory, the quantized system consists of both the atom and the electromagnetic field. The electromagnetic field is handled as an integral part of the system, not a perturbation, and it is considered quantum mechanically, not classically.

Exact solutions of the Schroedinger equation are possible for some systems of atomic levels and polarizations. It is particularly interesting that the stationary states of the total Hamiltonian of the dressed atom no longer correspond to a fixed, well defined number of photons in the field. The number states $|n\rangle$ for the pure radiation field are no longer eigenstates of the total Hamiltonian. In addition, it can be shown that stationary solutions exist which are a superposition of one or more of the atomic states calculated in the absence of fields and one or more of the number states of the field. This theory was used to predict the sideband intensities of well-known atomic transitions which were modulated by the application of optical or rf fields states. The "dressed state" theory predicted sideband intensi-

ties as functions of the interaction energy (or field strength) very successfully. It is reasonable to inquire whether the same formalism could be adapted to the analogous case in nuclei.

Maxwell's equations, which govern the interaction and propagation of electromagnetic fields, are linear and may be solved in terms of a Fourier decomposition. Magnetization is a more complex phenomenon, and it is expected that the solutions to the Landau-Lifshitz equation for obtaining $\vec{M}(t)$ will contain a number of harmonics of the frequency of the applied magnetic field. Each of these harmonics may then be considered to be an independent "dressing field" in the sense that Cohen-Tannoudji uses the term. If done in this way, the results should be summed over the harmonics which appear.

With this approach in mind, an extensive study was made of the publications concerning the dressed atom. The most comprehensive treatise was written by S. Haroche and published in *Annales de Physique* in 1971 in French. The results of the literature search were condensed into an internal document titled "The Interaction of the Dressed Atom", copies of which are available upon request.

As before, a better understanding of the magnetization is required before this approach could be adapted. The next sections describe models of how the direction of the magnetization varies as a function of time.

3) Development of the Coherent Switch Model of the Magnetization M(t) by Integrating the Landau-Lifshitz Equation

As mentioned in the previous sections, both the extension of the early DePaola and Collins model and the dressed state theory

of Cohen-Tannoudji are critically dependent upon the use of a good approximation to the complex precession of the magnetization vector, $\vec{M}(t)$ under the influence of an applied rf field. This section describes an investigation of the solutions to the Landau- Lifshitz equation appropriate to a thin ferromagnetic foil immersed in an rf magnetic field.

There are many solutions in the literature to the Landau-Lifshitz equation that describe static domain walls for various configurations of the magnetization[3,11,12]. The domain walls in an ^{57}Fe foil of the type generally used in experiments are expected to be "180^{o}" walls, that is walls in which the magnetization rotates through 180^{o} as the wall is traversed from one side to the other. There are fewer models of moving domain walls[3,12] than static walls. The precursive model of the demagnetizing field developed by DePaola and Collins to describe the magnetic fields interacting with the nuclear moment was taken from Chen[12]. He had described the concept of the magnetization rotating under the influence of the demagnetizing field which in turn is due to the magnetic poles developed when the applied magnetic field causes the magnetization to precess out of its initial plane. Thus a moving domain wall is formed. This was the model presented by DePaola and Collins[2]. On the other hand, there is no reason to expect the foil to be a single domain with only one moving domain wall.

Experimentally, it has been found that the static spectrum of the ^{57}Fe foil with no applied rf field demonstrates the usual six hyperfine lines. The relative intensities of the parent

lines in this case suggest that the magnetic field causing the splitting (the magnetization) is confined to the plane perpendicular to the transmission axis, that is, the plane of the foil. When an rf magnetic field is applied, the spectrum becomes much more complex. There are the usual six hyperfine lines (parent lines) plus six systems of sidebands, that is, absorption lines displaced from the parent line by frequencies corresponding to an integer (positive or negative) number times the applied frequency. The relative intensities of the parent lines continue to suggest that the magnetic field remains confined to the plane perpendicular to the transmission axis.

Thus, the internal magnetic structure of the ^{57}Fe foil is considered to be a composite of many platelet-shaped microcrystals with the platelets aligned more or less parallel with the plane of the foil. Demagnetizing fields develop in the volume of the platelets due to the appearance of magnetic poles on the surfaces. Each microcrystal or platelet is considered to be a single domain. In the coherent switching model, the magnetization at all points within the domain rotates in phase, that is, together as a unit without the usual domain wall where the rotation is concentrated within the wall. Since the platelets are not identical, there are discontinuities in the magnetization between the platelets, but inside the platelet, the magnetization is uniform. A second mode which includes the effects of the traversal of a domain wall through a nuclear site will be considered in section 4.

Equation (2) describes the motion of $\vec{M}$ under the influence of the four magnetic fields real and fictitious mentioned

previously. The problem was solved using a combination of spherical polar coordinates and the Cartesian components of $\vec{M}(t)$ as shown in Figure 8. The Cartesian components of $\vec{M}(t)$ are

$$M_x = M_s \sin\theta \cos\phi \tag{34a}$$

$$M_y = M_s \sin\theta \sin\phi \tag{34b}$$

$$M_z = M_s \cos\theta \quad . \tag{34c}$$

These four fields, the applied field, the magnetostatic field, the anisotropy field, and the exchange field, will each be considered as part of this model.

A) The Applied Field. Consistent with the initial conditions, the applied magnetic field is written as

$$\vec{H}_{app}(t) = - H_1 \sin \omega_1 t \quad . \tag{35}$$

B) The Magnetostatic Field. The Magnetostatic field is given by

$$\vec{B} = \mu_o(\vec{H} + \vec{M}) \tag{36}$$

where $\vec{H}$ is given by the solution to the Poisson equation

$$\vec{H} = (1/4\pi) \text{ grad } \int_V \frac{\text{div } \vec{M}}{r_{ij}} dV + \int_S \frac{\vec{M}\cdot\hat{n}}{r_{ij}} dS \tag{37}$$

The distance between the point of integration, i surrounded by the volume of integration dV, and the point j, at which $\vec{H}$ is to be evaluated, is denoted by r_{ij}. The first integral is taken throughout the entire volume of the magnetized body. The second integral is taken over the entire surface of the magnetized body, $\hat{n}$ being the inwardly directed unit vector normal to the surface.

The magnetostatic field is best considered on a case-by-case basis. The divergence of a vector field is a measure of the "sources" or "sinks" of that vector within a volume. Since the

magnitude of $\vec{M}$ remains the same throughout the body. div $\vec{M}$ = 0. The first integral resembles the volume integration of a charge density equal to div $\vec{M}$ which vanishes throughout the volume.

The second integral resembles an integration of a surface charge density over a surface. The non-zero magnetic pole density arises from the discontinuity of $\vec{M}$ at the surface and the continuity boundary requirement on $\vec{B}$ and $\vec{H}$. If $\vec{M}$ has a component normal to the surface, the magnetic pole density is $(\vec{M}\cdot\hat{n})$ on the surface. As the applied magnetic field increases parallel to the x axis, the magnetization begins to precess about the applied field, and $\vec{M}(t)$ moves out of the xy plane. A magnetic pole density develops on the faces of the foil parallel to the xy plane (boundary conditions on $\vec{B}$ and $\vec{H}$). These magnetic poles, whose density is given by $- M_z(t)$, are the source of the magnetostatic field, which then simplifies to the single term,

$$\vec{H}_d(t) = - \vec{M}_\perp = - M_s \cos\theta \, \hat{e}_z . \qquad (38)$$

C) The Anisotropy Field. The ferromagnetic foil is assumed to consist of many small microcrystals shaped like platelets or "microfoils". This is consistent with the amplitude distribution of the observed six-line spectrum in the absence of any applied field which is a rather sensitive function of the average orientation of the magnetization of each domain in the sample.

A magnetic material is said to have an easy or preferred direction of magnetization if a minimum energy state is obtained by having the magnetization lying along this easy direction. In a uniaxial material (the approximation used for each platelet of the ferromagnetic foil), any deviation of $\vec{M}(t)$ away from the easy

direction by an angle $(\phi-\phi_o)$ results in an increase in the energy density which may be accurately represented[3] by the expression $K_u \sin^2(\phi-\phi_o)$. The anisotropy constant K_u has units of energy/volume.

The effect of anisotropy is often represented[3] by an equivalent (but fictitious) magnetic field which lies along the easy direction of the crystal. The exchange field and the anisotropy field are derived in the same way: the expression for the interaction energy is derived from basic principles and then a fictitious magnetic field is deduced which yields the same functional expression for the energy, based on the relation,

$$E_{int} = -(1/2)\ \mu_o \vec{M}\cdot\vec{H}. \qquad (39)$$

A unit vector in the direction of the easy axis, as shown in Figure 8, is designated $\hat{e}_{x'}$. Thus the anisotropy field is given by

$$\vec{H}_a = Q\ (\vec{M}\cdot\hat{e}_{x'})\ \hat{e}_{x'} = Q\ M_s \sin\theta \cos(\phi-\phi_o)\ \hat{e}_{x'}. \qquad (40)$$

where

$$\hat{e}_{x'} = \cos\phi_o\ \hat{e}_x + \sin\phi_o\ \hat{e}_y \qquad (41)$$

and where $Q = (2K_u/\mu_o M_s^2)$ is a parameter of the crystal. The angle ϕ_o is the acute angle between the easy axis and the x axis of the foil coordinates.

D) The Exchange Field. Since the magnetization at every point within the domain precesses in the same manner, that is, in the domain where

$$\vec{M}(\vec{r},t) = \vec{M}(\vec{r}+\vec{dr},t)\ . \qquad (42)$$

the exchange field is zero. However, in materials where $\vec{M}$ depends on the position of the point of observation, such as in a

Landau-Lifshitz wall, the "exchange field" (fictitious) is given by

$$\vec{H}(\vec{r},t) = (2A/\mu_o M_s^2)\ \nabla^2\ \vec{M}(\vec{r},t) \qquad (43)$$

where A is a constant of the material.

The total magnetic field $\vec{F}$ in equation (2) is the sum of the fields given in equations (35), (38) and (40):

$$\vec{F} = \mu_o\ (\vec{H}_{app} + \vec{H}_d + \vec{H}_a) \quad . \qquad (44)$$

The equations of motion of the components of $\vec{M}(t)$ can be reduced and combined to yield equations for $d\phi/dt$ and $d\theta/dt$ in terms of the components of $\vec{F}$.

$$\begin{aligned} \sin\theta\ (d\phi/dt) = &- |\gamma| F_x\ [\ (\lambda/M_s)\sin\phi + \cos\phi\cos\theta] \\ &+ |\gamma| F_y\ [\ (\lambda/M_s)\cos\phi - \sin\phi\cos\theta] \\ &+ |\gamma| F_z \sin\theta \end{aligned} \qquad (45)$$

$$\begin{aligned} (d\theta/dt) = &- |\gamma| F_x\ [\ \sin\phi - (\lambda/M_s)\cos\phi\cos\theta] \\ &+ |\gamma| F_y\ [\ \cos\phi + (\lambda/M_s)\sin\phi\cos\theta] \\ &- |\gamma| F_z\ (\lambda/M_s)\ \sin\theta \end{aligned} \qquad (46)$$

The components of the total magnetic field $\vec{F}$ are given below.

$$F_x = -\mu_o H_1 \sin\omega_1 t + \mu_o M_s Q \sin\theta \cos(\phi-\phi_o) \cos\phi_o \qquad (47a)$$

$$F_y = +\mu_o M_s Q \sin\vartheta \cos(\phi-\phi_o) \sin\phi_o \qquad (47b)$$

$$F_z = -\mu_o M_s \cos\theta \qquad (47c)$$

These are first order differentials in time but very complicated functions of the angles θ and ϕ. A program was written in FORTRAN for the Hewlett-Packard Series 3000/560 Computer in which the angles θ and ϕ were built up in small steps from the initial conditions to obtain the magnetization $\vec{M}(t)$. An example solution is shown in Figure 9A.

The motion of $\vec{M}(t)$ seen in Figure 9A is quite consistent with the expectations reached by purely qualitative arguments. At t=0, the magnetization lies in the plane of the foil at $\theta_0 = \pi/2$ radians along the easy axis at an initial angle ϕ_0, assumed to be 0.35 radian in this example. The initial angles θ_0 and ϕ_0 are solution parameters. As the magnetostatic field increases through the precession of $\vec{M}(t)$ out of the xy plane, the effect of the magnetostatic field (in the z direction) completely dominates the motion of $\vec{M}(t)$, causing it to rotate in the xy plane rapidly until it nears the easy axis. After $\sin \omega_a t$ reaches its maximum and begins to decrease, the M_z begins to decrease as $\vec{M}(t)$ returns to the xy plane. The magnetization now lies along the easy axis but antiparallel to its initial direction. The motion of $\vec{M}(t)$ proceeds in a similar manner through the second half cycle of the applied field (although the motion is rotated about the z axis through 180° from its initial position).

The angle $\phi(t)$ as a function of time is also shown in Figure 9A. The oscillations of $\vec{M}(t)$ about the equilibrium position between the easy direction and the direction of the applied field are clearly shown. When $\vec{M}(t)$ switches, it is carried past its equilibrium position. The second term of equation 2 behaves as a restoring force which brings $\vec{M}(t)$ more nearly parallel to the equilibrium direction. The equilibrium direction is determined by the local minimum of the sum of the interaction energies of the magnetization with the anisotropy field and with the applied field. If the applied field were very strong, in time the restoring force would bring the magnetization parallel to the applied field. Figure 9B, which is from Takazumi's book[1], tends

to confirm this initially surprising result.

Figures 10A and 10B show the dependence of the motion of $\vec{M}(t)$ on the initial value of the angle θ for the values of θ_o equal to 91^o and 89^c, respectively. From these figures it is evident that the starting value of θ_o determines the direction of the initial rotation only. After the initial cycle, the behavior of $\vec{M}(t)$ is the same in all three cases. Since the magnetization is expected to lie in the plane of the foil (which minimizes the magnetostatic energy) only values near 90^o can be realistic. The maximum expected deviation from 90^o would be on the order of

$$\delta\theta_o \sim (\text{thickness of the foil/linear dimension of the foil})$$
$$\sim 5 \times 10^{-6} \text{ m} / 1 \times 10^{-2} \text{ m} \sim 0.03 \text{ degree} .$$

For this reason, an initial value of $\theta_o \sim 90^o$ is considered reasonable.

Finally, parameter studies have shown that for small values of H_1 and/or certain values of ϕ_o, the direction of magnetization in the foil does not switch. This is consistent with the picture above in that the applied field never develops enough interaction energy to overcome the effective anisotropy energy barrier, K_u.

The most important output of this model is the decomposition of sin $\phi(t)$ and cos $\phi(t)$ in terms of harmonics of the applied field frequency. The amplitudes of the harmonics then become the input to the program for solutions to the time dependent Schroedinger equation from which sideband intensities are computed according to one or another of the approaches being discussed. The amplitudes of the harmonic decompositions of cos $\phi(t)$ and sin $\phi(t)$ versus the order of the harmonic are shown in

Figure 11 for a typical set of input parameters.

Since this type of numerical integration of the Landau-Lifshitz equation must be condsidered "exact" to within the limits of numerical methods, its principal shortcoming is that coherence is limited to a single domain. The possible importance of domain walls is considered next. That is, this picture requires the magnetization of the entire domain to switch without the presence of a moving domain wall.

4) The Domain Wall Passage Model[3]

In the coherent switching model, magnetization within the domain is required to rotate uniformly (equation 42). It is also possible for the direction of the magnetization to change by means of passage of a domain wall through the material.

There are several different kinds of domain walls, for example the 90° wall where the direction changes by 90°, and the 180° wall between two domains whose magnetizations are antiparallel. An example containing a 180° wall is shown in Figure 12.

The position and shape of a domain wall is determined by the minimization of all the interaction energies. In the absence of an applied magnetic field, the domain walls remain static. When a magnetic field is applied, the domain wall moves in such a way that the volume of the domain whose magnetization is parallel to the applied field increases. The static and moving domain walls will be discussed next.

A) The Static Domain Wall.

Within the domain wall, the direction of $\vec{M}$ rotates while its magnitude remains fixed at the saturation value M_s.

The fundamental equation of micromagnetics states that the torque, given by the vector product of the magnetization and the total magnetic field, must vanish at every point in a medium which is in magnetostatic equilibrium. That is,

$$(\vec{M} \times \vec{F}) = 0. \tag{48}$$

For an infinitely long sample, the $\vec{H}$ field calcaulated from equation (37) is neglible. Since the magnitude of $\vec{M}$ remains constant, the divergence vanishes. There is no normal component of $\vec{M}$ at the surface of the sample, except either on faces which are far removed in the z direction from the point of observation or at the very small area where the domain wall meets the surface. Therefore, the contribution to $\vec{F}$ from the magnetostatic field is simply $\mu_o\vec{M}$ by equation (37).

However, since $\vec{M}$ is not uniform within the wall, there is a contribution from the exchange field. The easy direction of magnetization is taken to be parallel to the z axis. The components of $\vec{F}$ are

$$F_x = -(2K_u/M_s^2)\, M_x + (2A/M_s^2)\, \nabla^2 M_x + \mu_o M_x \tag{49a}$$

$$F_z = (2A/M_s^2)\, \nabla^2 M_z + \mu_o M_z \quad . \tag{49b}$$

In this case there is assumed to be no applied magnetic field, so that $H_{app} = 0$. The equation determining the spatial dependence of $\vec{M}$ is obtained by substituting equations (49a) and (49b) into equation (48),

$$\frac{A}{M_s^2}\left(M_z \frac{d^2M_x}{dy^2} - M_x \frac{d^2M_z}{dy^2}\right) - \frac{K_u}{M_s^2} M_z M_x = 0 \tag{50}$$

which is an ordinary differential equation since $\vec{M}$ is a function of y only. The components of $\vec{M}$ may be written

$$M_x = M_s \sin \theta \qquad (51a)$$

$$M_z = M_s \cos \theta \quad , \qquad (51b)$$

and the solution is found to be

$$\pm \tan(\theta/2) = \exp (y/\Delta) \qquad (52)$$

where Δ is the well known wall-width parameter,

$$\Delta = (A/K_u)^{1/2} \quad . \qquad (53)$$

One should note that the angle θ is that angle θ defined in Figure 12.

The choice of sign in equation (52) indicates that the domain wall may have either a clockwise or an anticlockwise screw-sense associated with the rotation of $\vec{M}$ in the xz plane. The components of $\vec{M}$ are

$$M_x = - M_s \tanh (y/\Delta) \qquad (54a)$$

$$M_z = \pm M_s \operatorname{sech} (y/\Delta) \quad . \qquad (54b)$$

B) The Moving Domain Wall.

In 1935 Landau and Lifshitz applied their equation [equation (2)] to the case of the motion of the static domain wall structure described above. They assumed that, although the wall was moving due to the influence of the applied magnetic field, the wall structure remained almost identical to its previous static structure [equations (54a) and (54b)]. That is, they assumed a "rigid wall structure".

If the wall moves as a rigid structure, then the spatial derivatives of $\vec{M}$ are defined. If the wall moves at a constant velocity, the time derivatives are defined as well. The problem

becomes algebraic and may be solved at any convenient point, such as the center of the domain wall. At the center of the domain wall, $M_x = M_s$ and $M_z = 0$. The other assumption which follows, once a rigid wall model is adopted, is that the anisotropy field and the exchange field remain antiparallel to $\vec{M}$ in the moving wall as in the stationary wall. Then only the applied field must be considered.

The domain on the left in Figure 13A is magnetized in the same direction as the applied field and consequently grows through the motion of the wall to the right with velocity v_y. This figure only shows $\vec{M}$ in the two domains and at the center of the wall, assuming a positive screw-sense of the rotation. Here only B_z enters into equation (37):

$$(dM_y/dt) = |\gamma| M_s B_z \qquad (55a)$$

$$(dM_z/dt) = |\gamma| \lambda B_z \quad . \qquad (55b)$$

The damping constant, λ, can only be determined experimentally by ferromagnetic resonance (FMR) on single crystal, spherically-shaped samples. In general[3], the dimensionless ratio (λ/Ms) has been found to be on the order of 10^{-3} or less. Since $(\lambda/M_s) \sim 10^{-3}$, equation (55a) is the more important of the two. This equation indicates that the proposal that the wall can move forward under the influence of the applied field must involve the vector $\vec{M}$ developing a component in the direction of motion. It is not possible to assume that the wall is really rigid and maintains exactly the same form which it has when stationary. As shown in Figure 13B, $\vec{M}$ must tilt by the angle ϕ to satisfy equation (55a).

At the center of the wall, the components of $\vec{M}$ are

$$M_x = M_s \cos \phi \tag{56a}$$

$$M_y = M_s \sin \phi \tag{56b}$$

$$M_z = 0 \quad . \tag{56c}$$

In the original development of the model, Landau and Lifshitz continued to assume that the contributions to $\vec{F}$ due to the exchange and anisotropy fields remain antiparallel to $\vec{M}$, as when $\phi=0$. The component M_z is assumed to have the same form as given in equation (54b). Then equation (37) is solved using only the magnetostatic field and the applied field.

$$-(dM_x/dt) = |\gamma| \sin \phi \, [B_z M_s - \lambda \mu_o M_s \cos \phi \sin \phi] \tag{57a}$$

$$+(dM_y/dt) = |\gamma| \cos \phi \, [B_z M_s - \lambda \mu_o M_s \cos \phi \sin \phi] \tag{57b}$$

$$+(dM_z/dt) = |\gamma| \, [\mu_o M_s^2 \cos \phi \sin \phi + \lambda B_z] \tag{57c}$$

From this, one sees that domain wall motion may be visualized as follows: as the wall moves forward, the vector $\vec{M}$ rotates about y. Since $\vec{M}$ has constant magnitude and ϕ is constant for a constant velocity, equations (57a) and (57b) are zero. The angle ϕ is related to the applied field B_z through

$$\sin 2\phi = (2B_z/\mu_o \lambda) \quad . \tag{58}$$

Since a rigid wall has been assumed, at the center of the wall

$$dM_z/dt = (\partial M_z/\partial y)(dy/dt) = (M_s/\Delta) \, v_y \quad . \tag{59}$$

which when combined with (57c) leads to an expression for v_y.

$$v_y = (|\gamma|\Delta/M_s)[\lambda B_z + \mu_o M_s^2 \sin \phi \cos \phi] \quad . \tag{60}$$

This gives the picture of a domain wall moving forward at a constant velocity v_y under the influence of a constant applied field B_z. Combining equations (58) and (60), the velocity is

given by

$$v_y = (|\gamma|\Delta M_s/\lambda)[1 + \lambda^2/M_s^2]\, B_z \quad . \tag{61}$$

In conducting materials where eddy currents complicate the calculations, it is possible to derive an expression for the domain wall velocity in terms of the product of a domain wall mobility and the applied field, that is,

$$v_y = \mu_w B_z \quad . \tag{62}$$

The domain wall mobility is given by

$$\mu_w = (\mu_o^2 \sigma M_s h)^{-1} \tag{63}$$

where σ is the conductivity and h is the thickness of the material.

From this domain wall velocity, a tilt angle ϕ could be deduced. If ϕ developed to approximately 45°, its maximum possible value, a significant amount of the magnetization field might be transmitted to an adjacent material. However, it was found that the passage of a wall at the surface transferred only on the order of 0.1 to 10.0 H_{app}, which was calculated to be at the most 20 gauss. Excitation of single non-magnetic stainless steel foils enriched with ^{57}Fe at this level failed to show sidebands. Thus it was concluded that the wall passage alone could not add significantly to the transfer of an effect from a magnetic to a non-magnetic foil at the level of magnitude seen in experiments.

In general, computer analyses of the static domain wall equations in conductors yield only solutions in which the magnetization remains parallel to the surface. A. Aharoni has made extensive analyses of domain walls in conducting materials, and his solution for a uniaxial material is shown in Figure 14.

These analyses reinforce the conclusion that the effects of moving domain walls in conductors are insufficient to transfer excitation to the non-magnetic foil. The problem of the transfer of sidebands from magnetic to non-magnetic layers lies at the focus of evolving concepts for the next year, but it must be recognized that such transfer leads to a relatively small effect, anyway. The largest effect, by an order-of-magnitude, is the development of sidebands in a single magnetic foil and this seems to be able to be described by the model synthesized from the previous approaches as described in the following section.

5) Solutions to the Time-dependent Schroedinger Equation at a Higher Level of Approximation

A more tractable approach to the solution of the time dependent Schroedinger equation discussed earlier was suggested by Professor Paul Berman of New York University. It is similar to some developed earlier but proves useful in more general cases for single foils.

In continued collaboration with Professor Berman, this approach has been programmed for the Hewlett-Packard Series 9000/560 Computer and is in the process of checkout. This approach combines the exact solution of the time dependent Schroedinger equation for the system of the ^{57}Fe nucleus in a ferromagnetic foil with perturbation theory solution of the absorption of the gamma-ray photon.

Figure 7 shows the energy levels and angular momentum assignments of the Mossbauer hyperfine transitions in ^{57}Fe. Before detailing the calculations, the matrix indices of the va-

rious states of the nucleus must be defined. To avoid the unnecessary complication of carrying both J and M_J as subscripts denoting a specific level, each magnetic sublevel of the ground state and excited state has been assigned a single index as follows:

1 is J = 1/2, M_J = +1/2 (ground state)

2 is J = 1/2, M_J = -1/2 (ground state)

3 is J = 3/2, M_J = +3/2 (excited state)

4 is J = 3/2, M_J = +1/2 (excited state)

5 is J = 3/2, M_J = -1/2 (excited state)

6 is J = 3/2, M_J = -3/2 (excited state)

The total Hamiltonian of the ^{57}Fe nucleus in a foil immersed in an rf magnetic field is given by

$$H = H_o + V_1(t) + V_2(t) \qquad (64)$$

where H_o is the nuclear Hamiltonian with $\vec{M}(t) = 0$ and no gamma ray interaction. The matrix H_o is

$$H_o = \left[\begin{array}{cc|cccc} 0 & 0 & 0 & 0 & 0 & 0 \\ 0 & 0 & 0 & 0 & 0 & 0 \\ \hline 0 & 0 & \hbar\omega_o & 0 & 0 & 0 \\ 0 & 0 & 0 & \hbar\omega_o & 0 & 0 \\ 0 & 0 & 0 & 0 & \hbar\omega_o & 0 \\ 0 & 0 & 0 & 0 & 0 & \hbar\omega_o \end{array}\right] \qquad (65)$$

In Eq. (64), $V_1(t)$ is the potential of the interaction of the magnetization $\vec{M}(t)$ with the nucleus having magnetic moment $\vec{\mu}_n$.

$$V_1(t) = -\vec{\mu}_n \vec{M}(t) = -g_x \mu_N \vec{M}(t) \cdot \vec{J} \qquad (66)$$

where g_x is the gyromagnetic ratio of the nuclear state x, μ_N is the nuclear magneton, and $\vec{J}$ is the vector total angular momentum operator.

The matrix $V_1(t)$ is given by

$$V_1(t) = \frac{\hbar\mu_N}{2}\left[\begin{array}{cc|cccc} g_g M_z & g_g M_- & 0 & 0 & 0 & 0 \\ g_g M_+ & g_g M_z & 0 & 0 & 0 & 0 \\ \hline 0 & 0 & 3g_e M_z & 3g_e M_- & 0 & 0 \\ 0 & 0 & 3g_e M_+ & g_e M_z & 2g_e M_- & 0 \\ 0 & 0 & 0 & 2g_e M_+ & -g_e M_z & 3g_e M_- \\ 0 & 0 & 0 & 0 & 3g_e M_+ & -3g_e M_z \end{array}\right] \quad (67)$$

The geometry is the same as shown in Figure 8. If $\vec{M}(t)$ has no z component, the diagonal elements of $V_1(t)$ vanish. The components of $\vec{M}(t)$ in the plane of the foil are

$$M_\pm = M_x(t) \pm i\, M_y(t) = M_s\, e^{\pm i\phi(t)} \quad . \quad (68)$$

The time dependence of the angle $\phi(t)$ is determined from the techniques described in Sections 3 and 4.

The coupling of the gamma ray field to the nucleus is given by $V_2(t)$. The selection rules for nuclear magnetic dipole transitions (M1 transitions) are $\Delta J = 0,\ 1$ and $\Delta M_J = \pm 1, 0$. The matrix $V_2(t)$ has the form

$$V_2(t) = \left[\begin{array}{cc|cccc} 0 & 0 & K_{13} & K_{14} & K_{15} & 0 \\ 0 & 0 & 0 & K_{24} & K_{25} & K_{26} \\ \hline K_{13}^* & 0 & 0 & 0 & 0 & 0 \\ K_{14}^* & K_{24}^* & 0 & 0 & 0 & 0 \\ K_{15}^* & K_{25}^* & 0 & 0 & 0 & 0 \\ 0 & K_{26}^* & 0 & 0 & 0 & 0 \end{array}\right] \quad (69)$$

where K_{jk} is the matrix element of the gamma ray absorption operator,

$$K_{jk} = \langle j | V_\gamma \cos \omega_\gamma t | k \rangle \quad . \quad (70)$$

The time dependent Schroedinger equation,

$$i\hbar\, (d\vec{a}/dt) = H\, \vec{a} \quad . \quad (71)$$

is written for this system as

$$i\hbar\,(d\vec{a}/dt) = (H_o + V_1(t) + V_2(t))\,\vec{a} \quad . \tag{72}$$

The problem can be divided into two parts. First, the time dependent Schroedinger equation is solved exactly for the Hamiltonian, $H = H_o + V_1(t)$. Then the solutions are used to treat $V_2(t)$ as a perturbation of the system.

First, the state of the system is transformed into the interaction representation,

$$\vec{a} = e^{-(iH_o t/\hbar)}\,\vec{b} \quad . \tag{73}$$

Explicitly,

$$a_k = b_k \qquad \text{for } k = 1,2 \text{ (ground state)} \quad ,$$

$$a_k = (e^{-i\omega_o t})\,b_k \qquad \text{for } k = 3,4,5,6 \text{ (excited state)}.$$

When equation (73) is substituted into equation (72), the equation for $(d\vec{b}/dt)$ becomes

$$i\hbar\,(d\vec{b}/dt) = (V_1' + V_2')\,\vec{b} \tag{74}$$

where the V' matrix is defined by

$$V' = e^{(iH_o t/\hbar)}\,V\,e^{-(iH_o t/\hbar)} \quad , \tag{75}$$

or

$$V'_{ij} = V_{ij}\,e^{(i\omega_{ij}t)} \tag{76a}$$

$$\omega_{ij} = (E_i - E_j)/\hbar \quad . \tag{76b}$$

Since $V_1(t)$ does not have matrix elements between the ground state and the excited state, $V'_1(t) = V_1(t)$.

However, $V_2(t)$ does have matrix elements linking the ground state to the excited state. The non-zero matrix elements of V_2' are

$$(V_2')_{13} = K_{13}\,e^{-i\omega_o t} = (V_2')^*_{31} \tag{77a}$$

$$(V_2')_{14} = K_{14}\,e^{-i\omega_o t} = (V_2')^*_{41} \tag{77b}$$

$$(V_2')_{15} = K_{15}\, e^{-i\omega_o t} = (V_2')^*_{51} \qquad (77c)$$

$$(V_2')_{24} = K_{24}\, e^{-i\omega_o t} = (V_2')^*_{42} \qquad (77d)$$

$$(V_2')_{25} = K_{25}\, e^{-i\omega_o t} = (V_2')^*_{52} \qquad (77e)$$

$$(V_2')_{26} = K_{26}\, e^{-i\omega_o t} = (V_2')^*_{62} \quad . \qquad (77f)$$

The gamma ray interaction may be written as

$$V_2 = V_\gamma \cos \omega_\gamma t = (1/2)\, V_\gamma\, (e^{i\omega_\gamma t} + e^{-i\omega_\gamma t}) \quad . \qquad (78)$$

The rotating wave approximation consists of neglecting all of the terms which contain the sum of the frequencies, $\pm(\omega_\gamma + \omega_o)$, in the exponential time dependence. In this approximation, the non-zero matrix elements of V_2' become

$$(V_2')_{13} = (V_\gamma)_{13}\, e^{i\Delta t} = (V_2')^*_{31} \qquad (79a)$$

$$(V_2')_{14} = (V_\gamma)_{14}\, e^{i\Delta t} = (V_2')^*_{41} \qquad (79b)$$

$$(V_2')_{15} = (V_\gamma)_{15}\, e^{i\Delta t} = (V_2')^*_{51} \qquad (79c)$$

$$(V_2')_{24} = (V_\gamma)_{24}\, e^{i\Delta t} = (V_2')^*_{42} \qquad (79d)$$

$$(V_2')_{25} = (V_\gamma)_{25}\, e^{i\Delta t} = (V_2')^*_{52} \qquad (79e)$$

$$(V_2')_{26} = (V_\gamma)_{26}\, e^{i\Delta t} = (V_2')^*_{62} \qquad (79f)$$

where the angular frequency Δ is defined by

$$\Delta = \omega_\gamma - \omega_o \quad . \qquad (80)$$

The matrix U(t) is defined as the V'_2 matrix in the rotating wave approximation as shown in equations (79a) through (79f) above. In the rotating wave approximation, equation (73) is rewritten,

$$i\hbar\,(d\vec{b}/dt) = (V_1 + U)\,\vec{b} \quad . \tag{81}$$

Furthermore, the vector $\vec{b}$ may be written as the matrix product

$$\vec{b} = \exp\{(i/\hbar)\int_0^t V_1(t')dt'\}\,\vec{c} \equiv T(t)\,\vec{c} \quad . \tag{82}$$

The equation of motion for the matrix T(t) is

$$i\hbar\,(dT(t)/dt) = V_1\,T(t) \tag{83}$$

with the initial condition, $T(t=0) = 1$, the unit matrix.

The equation of motion of the vector $\vec{c}$ is now given by

$$i\hbar\,(d\vec{c}/dt) = U'(t)\,\vec{c} \tag{84}$$

where U'(t) is defined by

$$U'(t) = T^{+}\,U(t)\,T \quad . \tag{85}$$

The matrix U'(t) has the same general form as V_2' shown above in equations (79a) through (79f). The ground states and the excited states are now mixed as a result of both V_1 and V_2. The relaxation effects of the natural decay of the excited state are now added into equation (84),

$$(d\vec{c}/dt) = (-i/\hbar)\,U'(t)\,\vec{c} - (1/2)\gamma\,\vec{c} \tag{86}$$

where the matrix γ is defined

$$\gamma = \left[\begin{array}{cc:cccc} 0 & 0 & 0 & 0 & 0 & 0 \\ 0 & 0 & 0 & 0 & 0 & 0 \\ \hdashline 0 & 0 & \gamma & 0 & 0 & 0 \\ 0 & 0 & 0 & \gamma & 0 & 0 \\ 0 & 0 & 0 & 0 & \gamma & 0 \\ 0 & 0 & 0 & 0 & 0 & \gamma \end{array}\right] \quad . \tag{87}$$

The quantity γ has the dimensions $(\sec^{-1})$ and is defined as the inverse of the natural lifetime of the excited state, $\gamma = (1/\tau)$.

The net absorption of the gamma rays is proportional to

$\sum_{m=3}^{6} |a_m(t)|^2$ for times $t \gg (2/\gamma)$. However,

$$\sum_{m=3}^{6} |a_m(t)|^2 = \sum_{m=3}^{6} |b_m(t)|^2 = \sum_{m=3}^{6} |c_m(t)|^2 \qquad (88)$$

since H_o and V_1 are Hermitian. The components of $\vec{c}(t)$ are given by

$$c_j(t) = (-i/\hbar) \sum_{k=1}^{2} \int_0^t U'_{jk}(t') \, e^{(-\gamma/2)(t-t')} \, c_k(t') \, dt' . \qquad (89)$$

For $t \gg (2/\gamma)$, the absorption is proportional to

$$\langle \sum_{k=3}^{6} |c_k(t)|^2 \rangle \quad ,$$

where the time average is taken over the time response of the detector. This completes the formal solution.

If the decay of the excited state into the ground state is neglected, then to the zeroth order in $V_2(t)$,

$$c_k \simeq c_k(0) \qquad k = 1,2 \qquad (90)$$

since $V_2(t)$ does not couple the ground states, 1 and 2, in the first order. Furthermore, since H_o and V_1 are Hermitian, the amplitude $c_k(t)$ for the ground states may be written

$$c_k(t) = c_k(0) = a_k(0) \quad \text{for } k = 1,2 \quad . \qquad (91)$$

The ground state splitting is small compared to the thermal energy at room temperature, so that the ground states are equally populated. Thus,

$$a_k(0) = (1/\sqrt{2}) \qquad \text{for } k = 1,2 \quad . \qquad (92)$$

The absorption spectrum then becomes the result of six computational steps.

Step 1: To determine the $V_1(t)$ matrix given by equations (67), equation (68) may be expanded to

$$M_{\pm} = M_s \, (\cos \phi(t) \pm i \sin \phi(t)) \quad . \qquad (93)$$

The output of the program written for the coherent switching

model described above includes the Fourier decomposition amplitudes A_n, B_n, A'_n, and B'_n, where

$$\cos \phi(t) = \sum_{n=0}^{\infty} [A_n \cos n\omega_1 t + B_n \sin n\omega_1 t] \qquad (94)$$

$$\sin \phi(t) = \sum_{n=0}^{\infty} [A'_n \cos n\omega_1 t + B'_n \sin n\omega_1 t] \quad . \qquad (95)$$

These amplitudes may be used as inputs which specify $V_1(t)$.

Step 2: Step 2 is the numerical solution of equation (83) for the matrix T(t) subject to the initial condition, T(t=0) = 1. Equation (83) is a first order differential equation for the matrix T(t). Since the elements of the matrix (dT(t)/dt) are known, the elements of T(t) are integrated numerically from the initial values specified at t=0.

Step 3: With the elements of T(t) tabulated as a function of time, the elements of U'(t) are calculated as a function of time. The matrix $U'(t) = T^+ U T$ (equation 85) is formed for a given gamma-ray frequency ω_γ.

Step 4: The integral of equation (89) is numerically computed as a function of time, the magnitude squared, and then the summation over the indices of the excited states is taken. The calculation of $\langle \sum_{k=3}^{6} |c_k(t)|^2 \rangle$ as a function of time is taken for this value of ω_γ.

Step 5: This summation is averaged over a time comparable to several natural lifetimes.

Step 6: Steps 1 through 5 are repeated for another value of ω_γ until the spectrum has been covered.

A program which performs steps 1 through 3 has been written and is in the process of checkout. Since these equations are quite complicated, a simple case was chosen which could also be verified without resorting to numerical analysis. This is the static case where $\vec{M}(t) = M_s \hat{e}_x$ or $\phi = 0^\circ$. The magnetization lies in the xy plane, so the diagonal elements of V_1 vanish.

With V_1 given, and the splittings of the ground and excited levels given by

$$g_g \mu_N M_s = - \hbar\omega_g \tag{96a}$$

$$g_e \mu_N M_s = + \hbar\omega_e \quad . \tag{96b}$$

the differential equations for the elements of T(t) are

$$i \dot{T}_{1j} = -(\omega_g/2)\, T_{2j} \tag{97a}$$

$$i \dot{T}_{2j} = -(\omega_g/2)\, T_{1j} \tag{97b}$$

$$i \dot{T}_{3j} = (\sqrt{3}/2)\omega_e\, T_{4j} \tag{97c}$$

$$i \dot{T}_{4j} = (\sqrt{3}/2)\omega_e\, T_{3j} + \omega_e\, T_{5j} \tag{97d}$$

$$i \dot{T}_{5j} = \omega_e\, T_{4j} + (\sqrt{3}/2)\omega_e\, T_{6j} \tag{97e}$$

$$i \dot{T}_{6j} = (\sqrt{3}/2)\omega_e\, T_{5j} \quad . \tag{97f}$$

The elements of the T matrix in this special case are found to be

$$T_{11} = \cos K_g x = T_{22} \tag{98a}$$

$$T_{12} = i \sin K_g x = T_{21} \tag{98b}$$

$$T_{33} = (1/4)\,[3 \cos K_e x + \cos 3K_e x] = T_{66} \tag{98c}$$

$$T_{34} = (-i/4)(\sqrt{3})\,[\sin K_e x + \sin 3K_e x] = T_{43} \tag{98d}$$

$$T_{35} = (1/4)(\sqrt{3})\,[-\cos K_e x + \cos 3K_e x] = T_{53} \tag{98e}$$

$$T_{36} = (+i/4)\,[3 \sin K_e x - \sin 3K_e x] = T_{63} \tag{98f}$$

$$T_{44} = (1/4)\,[\cos K_e x + 3 \cos 3K_e x] = T_{55} \tag{98g}$$

$$T_{45} = (i/4)\,[\sin K_e x - 3 \sin 3K_e x] = T_{54} \tag{98h}$$

$$T_{46} = (1/4)(\sqrt{3})\,[-\cos K_e x + \cos 3K_e x] = T_{64} \tag{98i}$$

$$T_{56} = (-i/4)(\sqrt{3})\,[\sin K_e x + \sin 3_e x] = T_{65} \qquad (98)$$

where, in terms of the parameters of the computer program,

$$x = \omega_1 t \qquad (99a)$$

$$K_g x = (\omega_g/2\omega_1)(\omega_1 t) = (\omega_g/2) \qquad (99b)$$

$$K_e x = (\omega_e/2\omega_1)(\omega_1 t) = (\omega_e/2) \quad . \qquad (99c)$$

All other $T_{ij} = 0$. That T is symmetric in this case is due to the choice $M_+ = M_- = M_s$. This is not the usual property of T.

The matrices T(t) and U'(t) have been calculated and compared with the functions above. There is very good agreement. Discrepancies are oscillatory in nature and do not seem to build up in time. The worst case deviations of U'(t) are about 0.3%.

Work continues on this approach with the next step being the checkout of each computational step.

SIGNIFICANCE

To dress an isomeric state requires a certain arrangement of nuclear levels that would make them undetectable to conventional techniques of nuclear spectroscopy. Our method of FMS is the only means found to date that can be used to search for this combination among the 29 best candidates.

In order to advance the theory of FMS during the current reporting period we have generated a computer program to integrate the Landau-Lifshitz equation for the foil geometry. Also we are in the process of completing the checkout of the program described in section 5 which theoretically predicts the sideband amplitudes when the time dependence of $\vec{M}(t)$, given by the solution of the Landau-Lifshitz equation, is known. Since this program is rather general, it can also be utilized to predict the Mossbauer absorption spectrum of other nuclear species embedded in the ferromagnetic foil, for example a Sn nucleus embedded in Fe. Further modifications of the program are planned to extend its capacity so that more general motions of $\vec{M}(t)$ may be incorporated.

The successes to date of the new FMS apparatus for nuclear spectroscopy indicate that a much higher resolution, by perhaps six orders of magnitude, can be achieved through a reasonable upgrade of the apparatus. If the range of tunability does extend to the ferromagnetic spin resonance (FSR) frequency, then it will be possible to construct a swept frequency device capable of continuously tuning over a range of 10^{11} linewidths, an enormous improvement in the state-of-the-art of nuclear spectroscopy.

REFERENCES

1. B. D. DePaola, S. S. Wagal and C. B. Collins, J. Opt. Soc. Am. B 2, 541 (1985).

2. C. B. Collins and B. D. DePaola, Optics. Lett. 10, 25 (1985).

3. T. H. O'Dell, Ferromagnetodynamics, Wiley, New York (1981).

4. S. Chikazumi, Physics of Magnetism, Wiley, New York (1964).

5. C. Cohen-Tannoudji, Cargese Lectures in Physics, Vol. 2, ed. by M. Levy, Gordon and Breach (1968).

6. C. Cohen-Tannoudji and S. Haroche, J. Physique, 30, 125 (1969).

7. C. Cohen-Tannoudji, Frontiers in Laser Spectroscopy, Session XXVII, North Holland Publishing Co. (1975).

8. S. Haroche, Annales de Physique, 6, 189, (1971).

9. S. Haroche, Annales de Physique, 6, 327 (1971).

10. L. D. Landau and E. M. Lifshitz, Quantum Mechanics, Pergamon Press, New York (1976).

11. A. Aharoni, J. Appl. Phys., 46, 1783 (1975).

12. C. Chen, Magnetism and Metallurgy of Soft Magnetic Materials, North Holland Publishing Co. (1977).

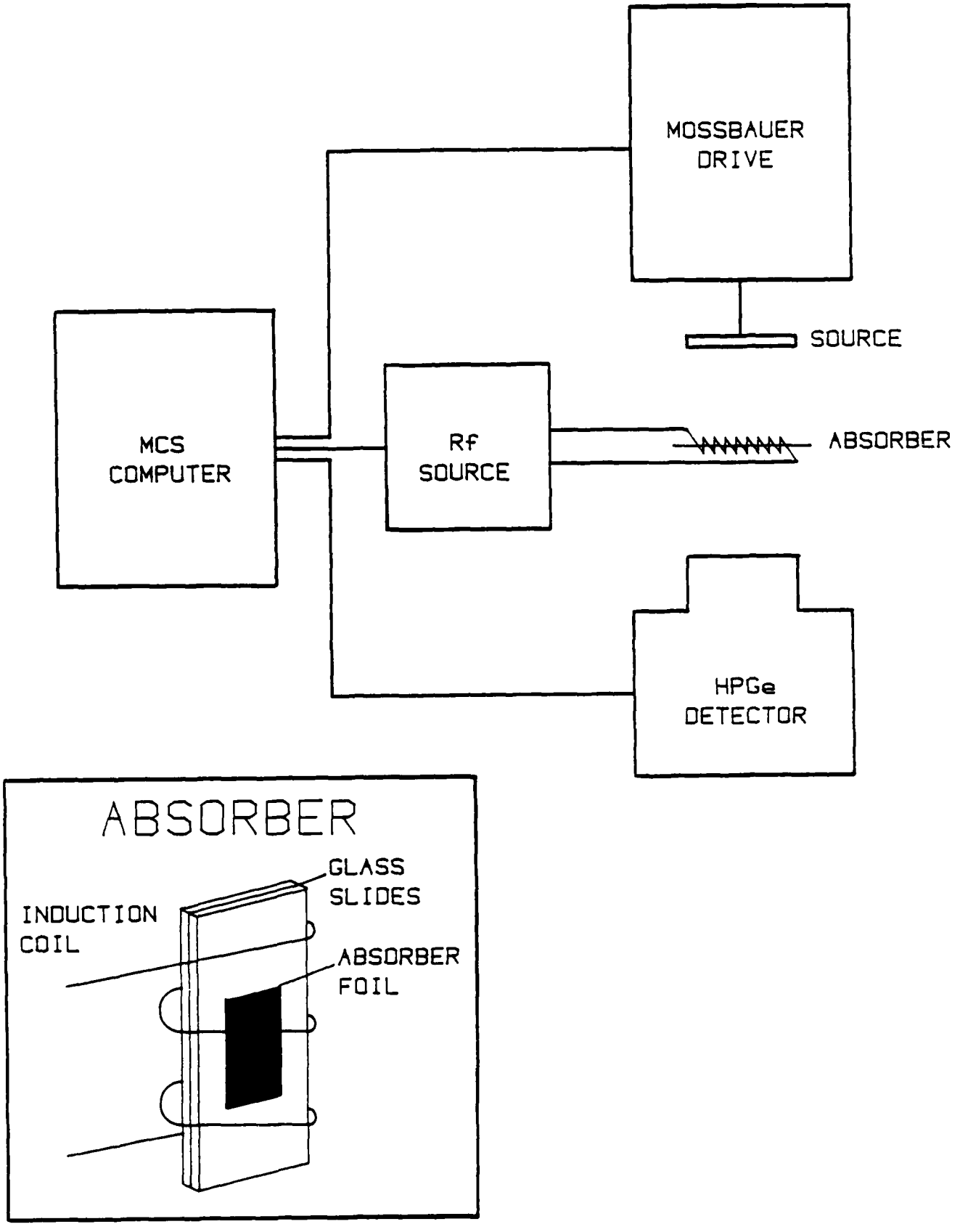

Figure 1. The heart of the Frequency Modulated Spectrometer (FMS) is a real time computer interface with a linear motor, an Rf signal generator, and a γ-ray detector. The γ-ray absorber, mounted in thin cover glass slides for rigidity, is subjected to an Rf alternating magnetic field. The computer scans through frequencies of the Rf field to obtain a spectrum.

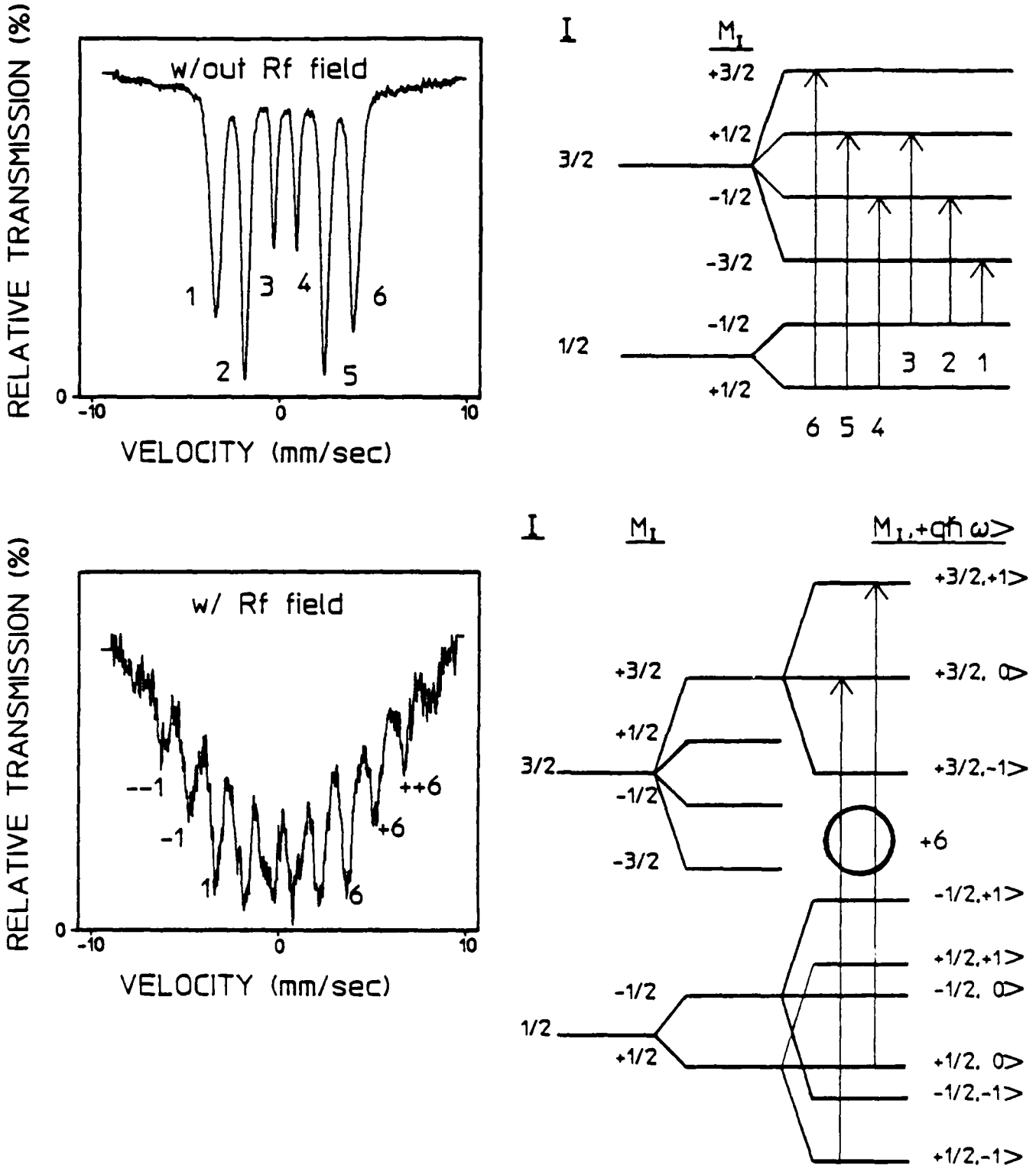

Figure 2. The effects of an alternating magnetic field on the hyperfine structure of ^{57}Fe are readily observable in conventional Mossbauer spectra. Without the Rf field there are 6 allowed transitions (parent transitions). The additional structure in the spectrum taken in the presence of the Rf field has the appearance of additional allowed transitions (sidebands).

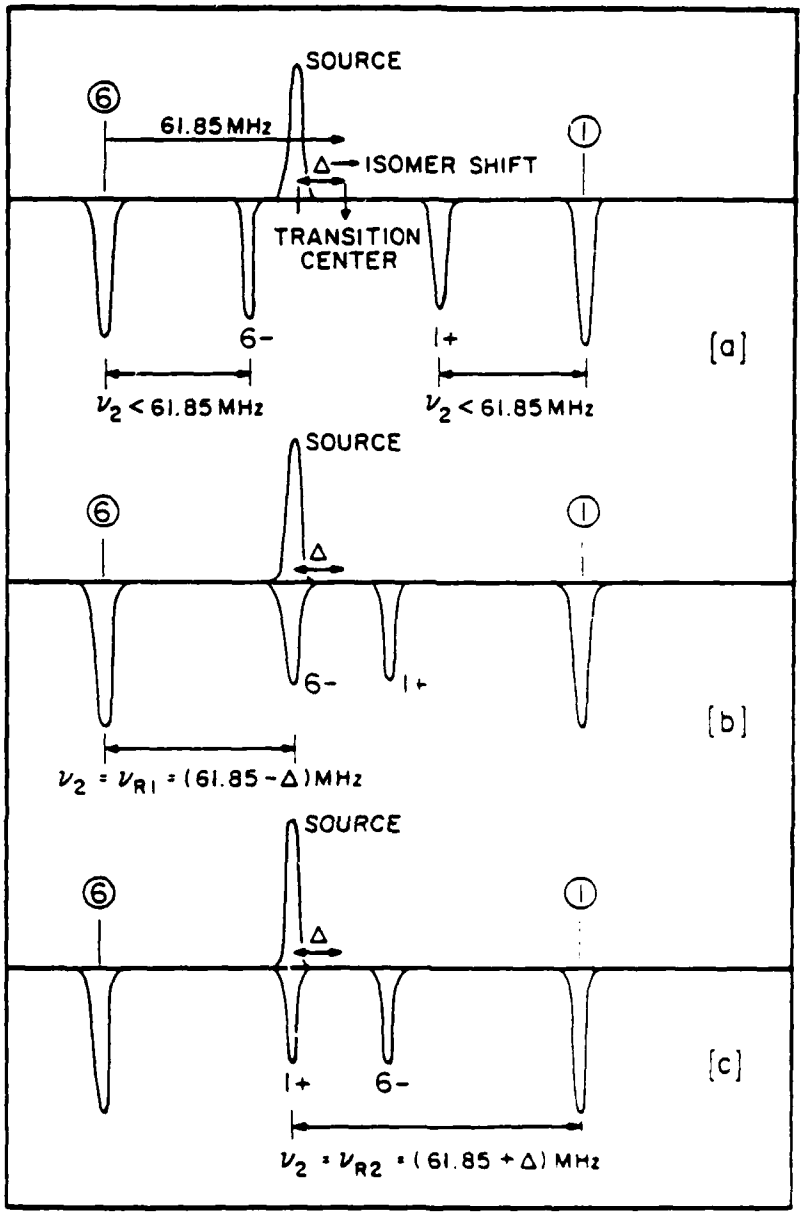

Figure 3. As the frequency of the rf field is increased, sidebands from symmetrically opposed transitions approach the transition center. For a stationary source, the probing radiation's energy is separated from the transition center by the isomer shift Δ between the source and absorber. Therefore, these two sidebands will move through the point of observation separated by twice the isomer shift.

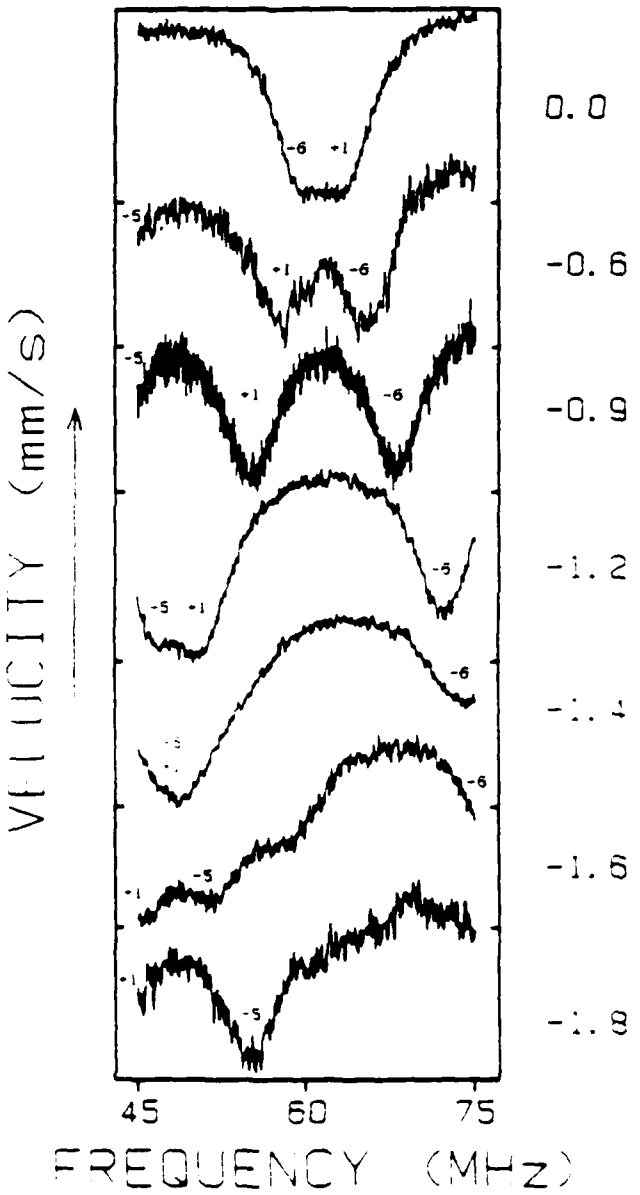

Figure 4. For a stationary source, the sidebands from the parent transitions 1 and 6 in ^{57}Fe overlap at 60 MHz separated by twice the isomer shift. If the source is given a small constant velocity, then the sidebands are separated by twice the isomer shift plus twice the velocity offset. At sufficiently high velocities a sideband from parent transition 5 comes within the frequency range scanned.

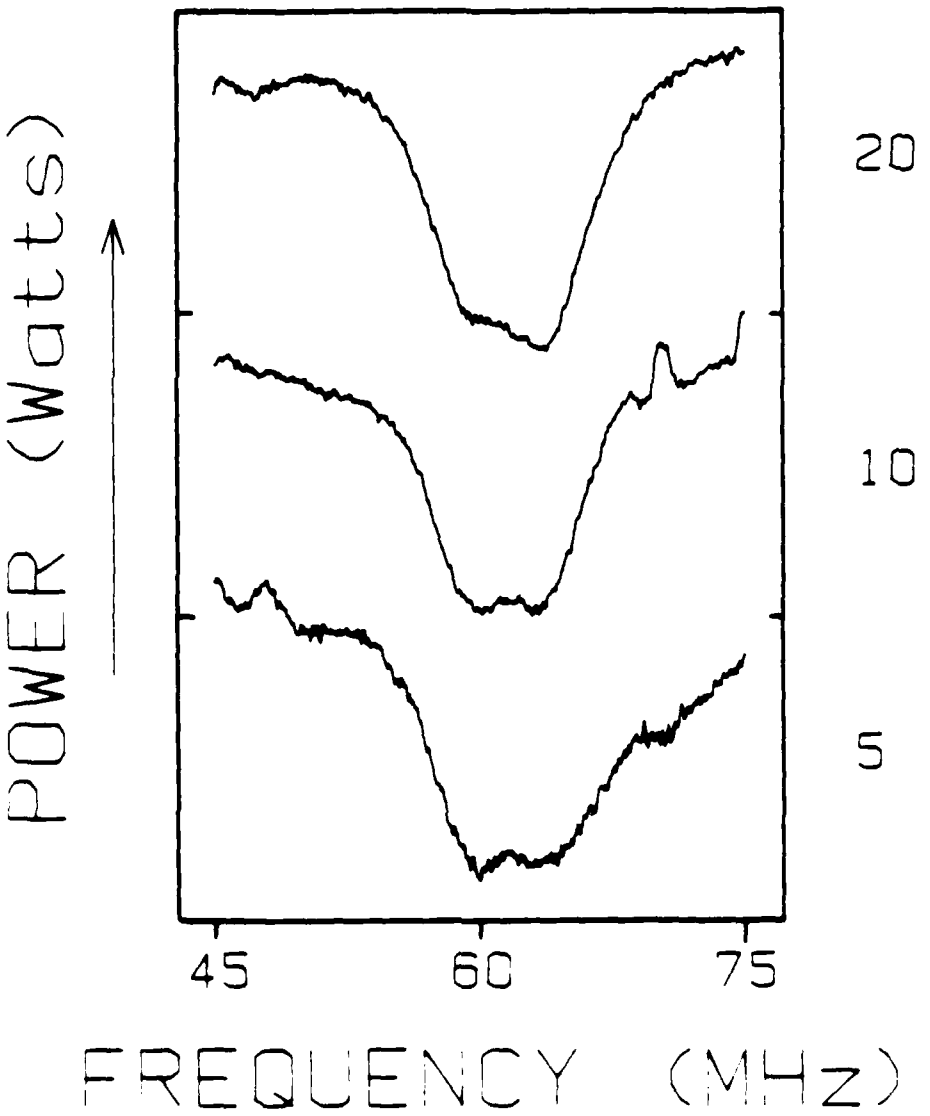

Figure 3. The amplitude of the sideband absorptions is dependent on the power of the applied RF field. These are EMR spectra taken at three different powers.

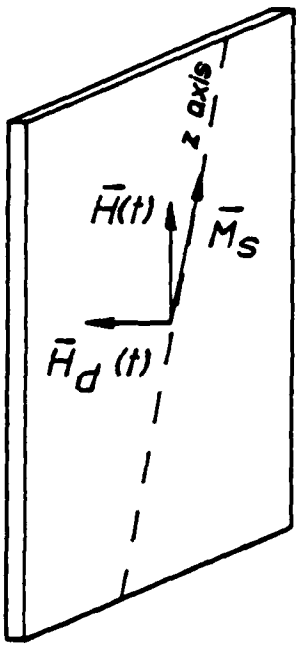

Figure 6. Primed coordinate system defined in the plane of the foil such that $\vec{M}$ always cooresponds to the z axis. The vector $\vec{H}_d$ is perpendicular to the plane of the foil.

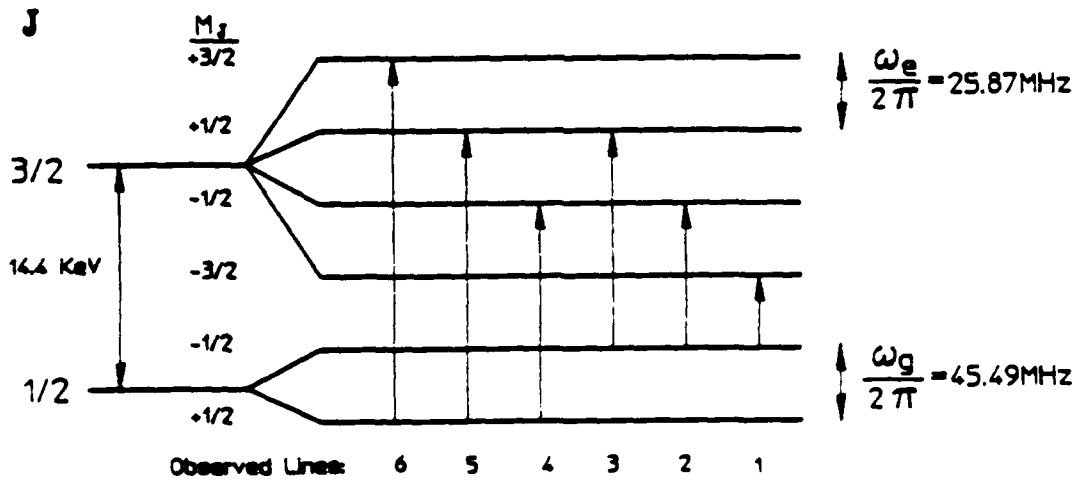

Figure 7. Energy levels of the Mossbauer transition of the ^{57}Fe nucleus in a ferromagnetic Fe foil indicating the total angular momentum, the magnetic sublevels, and the observed transitions.

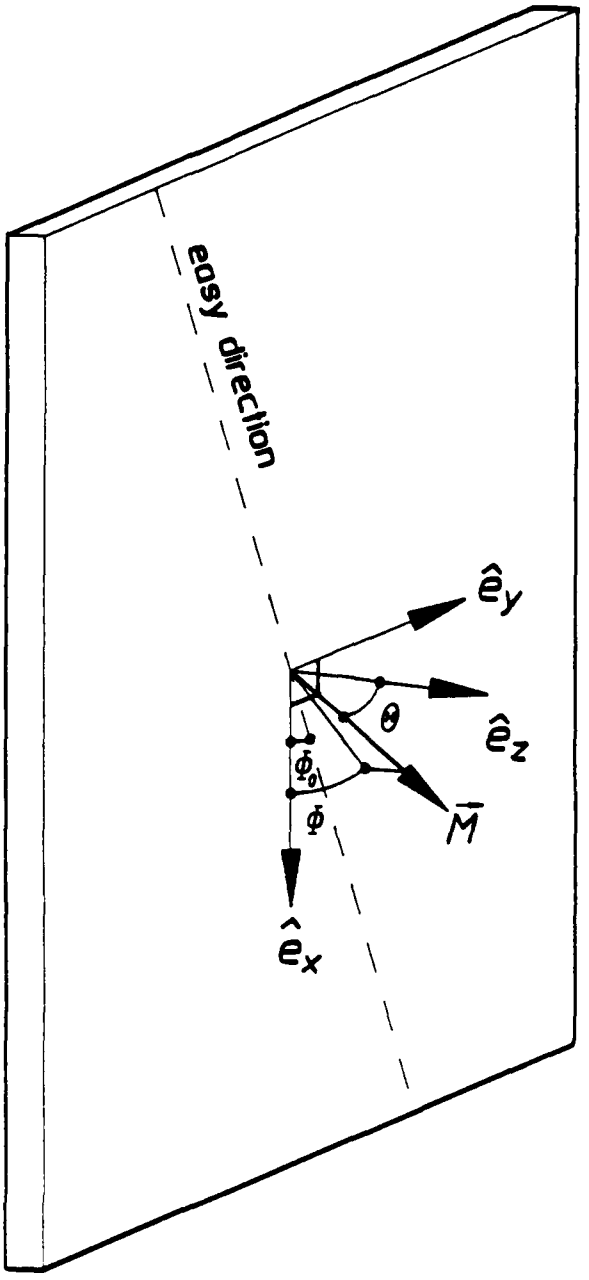

Figure 8. In the coherent switching model, coordinate system of the ^{57}Fe foil showing $\vec{M}(t)$ in relation to coordinates ϕ and θ. The foil lies in the xy plane.

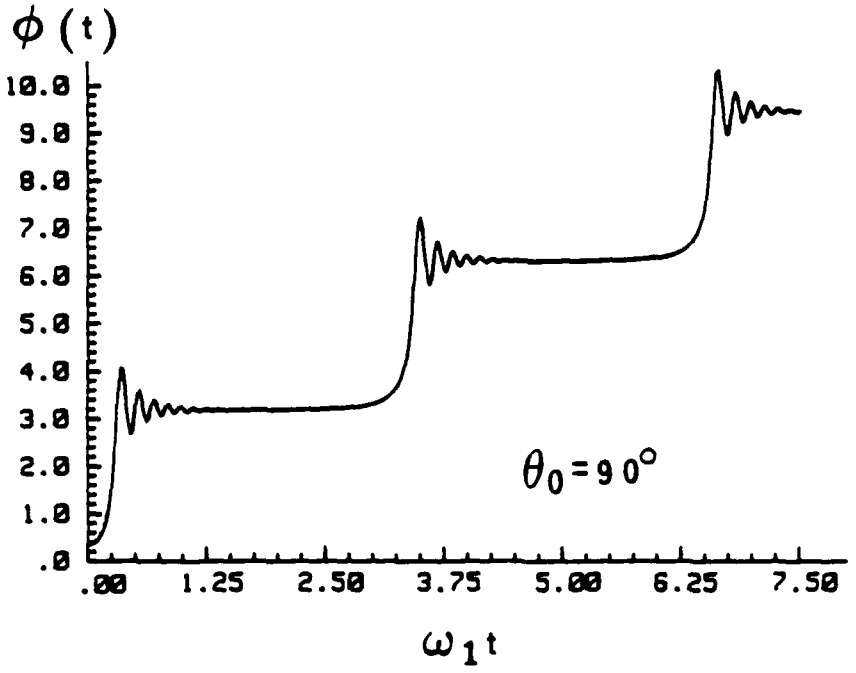

Figure 9A. Results of integrating the Landau-Lifshitz equation. $\phi(t)$ as a function of $(\omega_1 t)$, for the following initial conditions and input parameters:

Initial conditions: $\phi_o = 0.35$ rad $= 20^\circ$

$\theta_o = \pi/2$ rad $= 90^\circ$

Input parameters: $|\gamma| H_{app} = 33.61 \times 10^6$ rad/sec

$\omega_1 = 6\pi \times 10^7$ rad/sec ($\nu = 30$ MHz

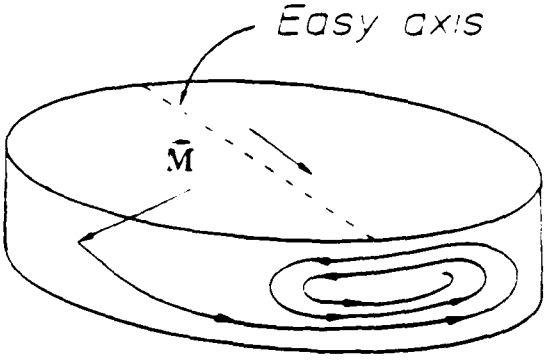

Figure 9B. The motion of the magnetization $\vec{M}(t)$ for a thin film switching. Adapted from Figure 16.13 of Physics of Magnetism by S. Chikazumi[4].

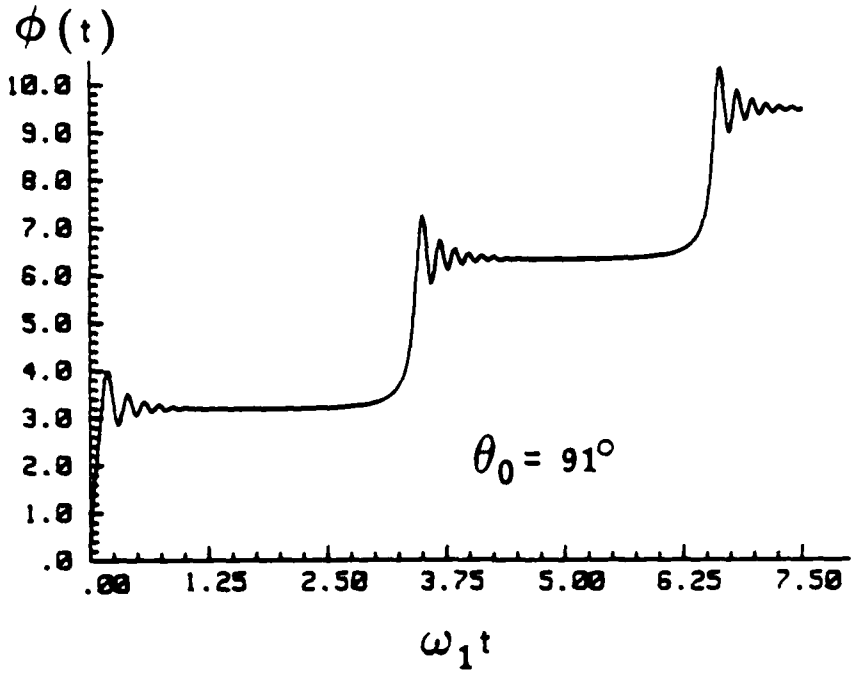

Figure 10A. Results of integrating the Landau-Lifshitz equation for $\theta_0 = 91^\circ$. All other parameters are the same as in Figure 9A.

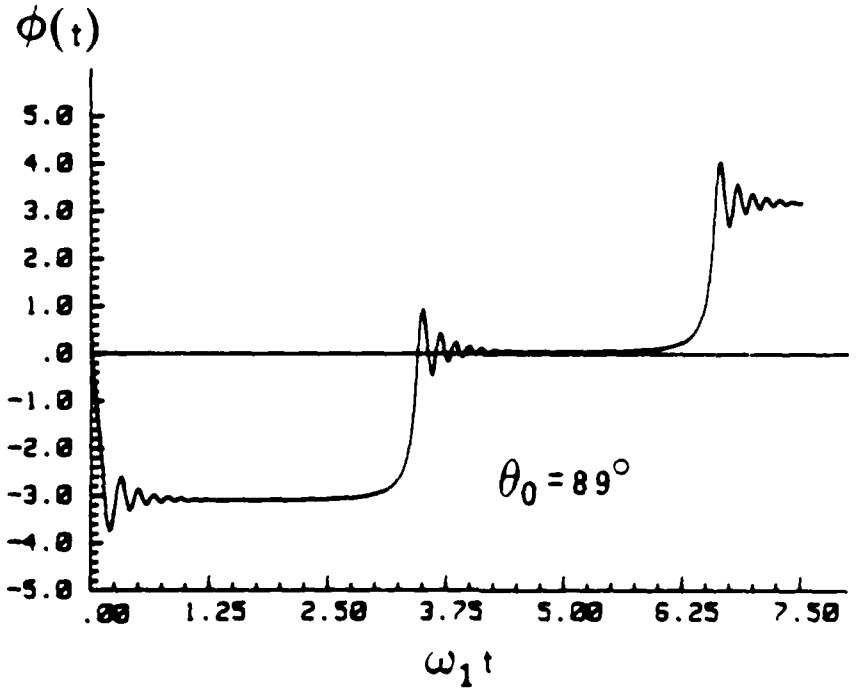

Figure 10B. Results of integrating the Landau-Lifshitz equation for $\theta_0 = 89^\circ$. All other parameters are the same as in Figure 9A.

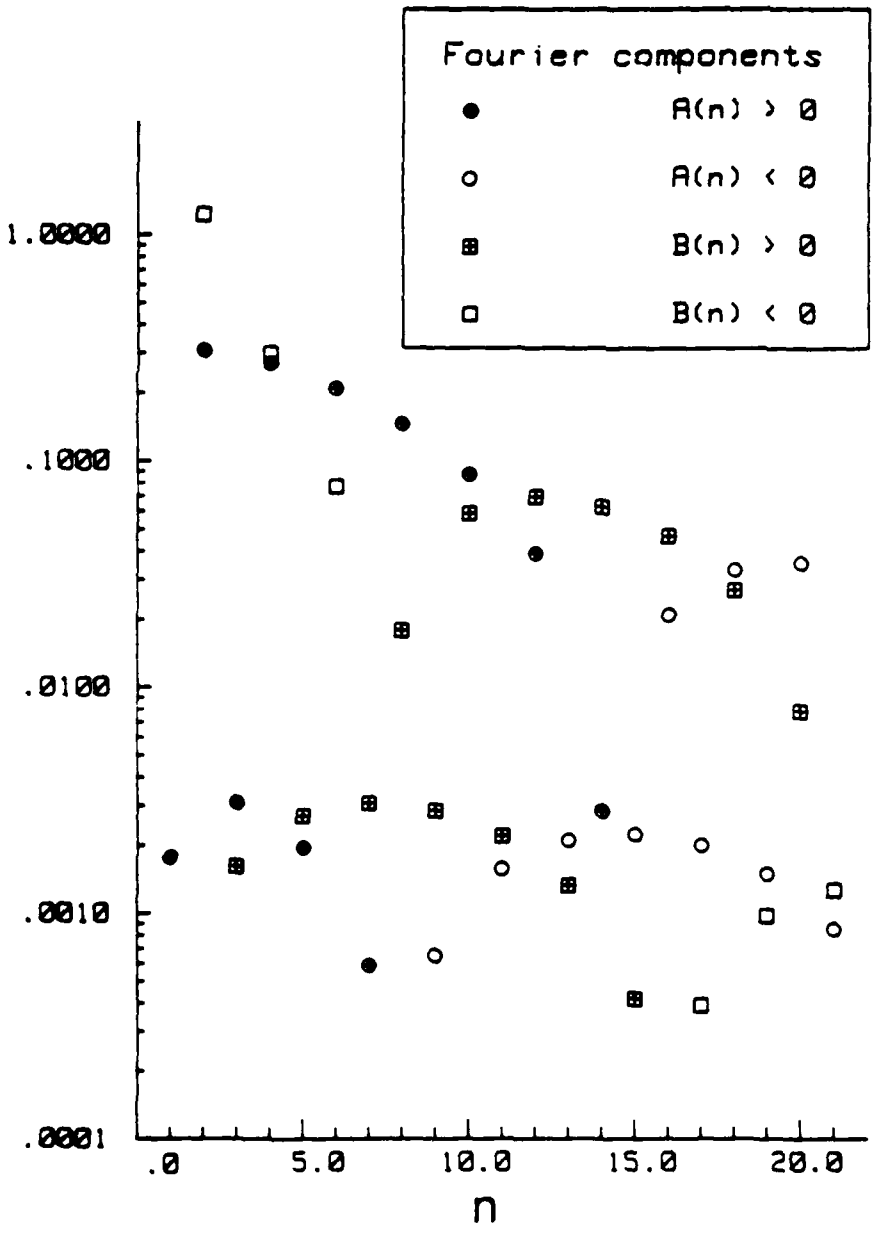

Figure 11. The Fourier decomposition of cos $\phi(t)$ derived from $\phi(t)$ as shown in Figure 9A according to the expansion

$$\cos \phi(t) = \sum_{n=0}^{\infty} [A(n) \cos n\omega_1 t + B(n) \sin n\omega_1 t].$$

The absolute values of the components A(n) and B(n) are plotted as functions of the order n. The sign of the component may be inferred from the legend.

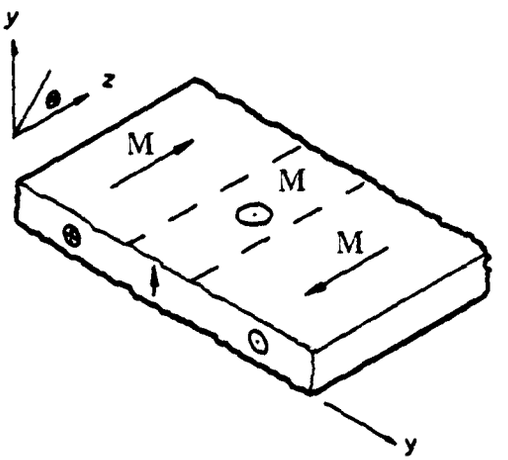

Figure 12. The magnetization $\vec{M}$ in a static Landau-Lifshitz 180° domain wall. When the magnetization lies in the plane, there is no surface divergence $(\vec{M}\cdot\hat{n})$ except over the small region where the domain wall cuts the surface. Adapted from Figure 2.2 of Ferromagnetodynamics by T. H. O'Dell[3].

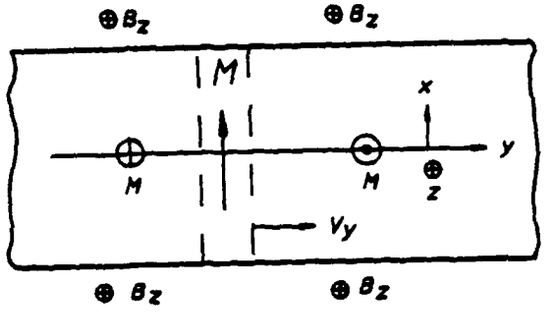

Figure 13A. Coordinate system for a "rigid" domain wall motion under the influence of an externally applied field B_z. Adapted from Figure 2.4 of Ferromagnetodynamics by T. H. O'Dell[3].

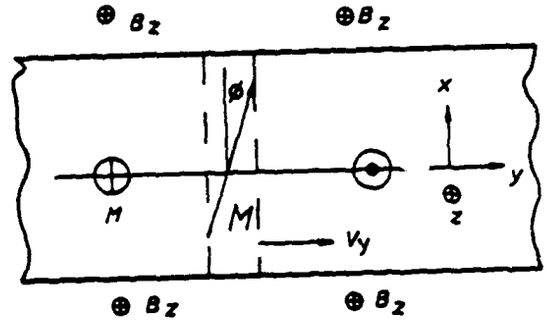

Figure 13B. Coordinate system for domain wall motion in which the magnetization is tilted slightly out of the xz plane. Analysis shows that the moving wall must develop a component of $\vec{M}$ which lies along the direction of motion. Adapted from Figure 2.5 of Ferromagnetodynamics by T. H. O'Dell[3].

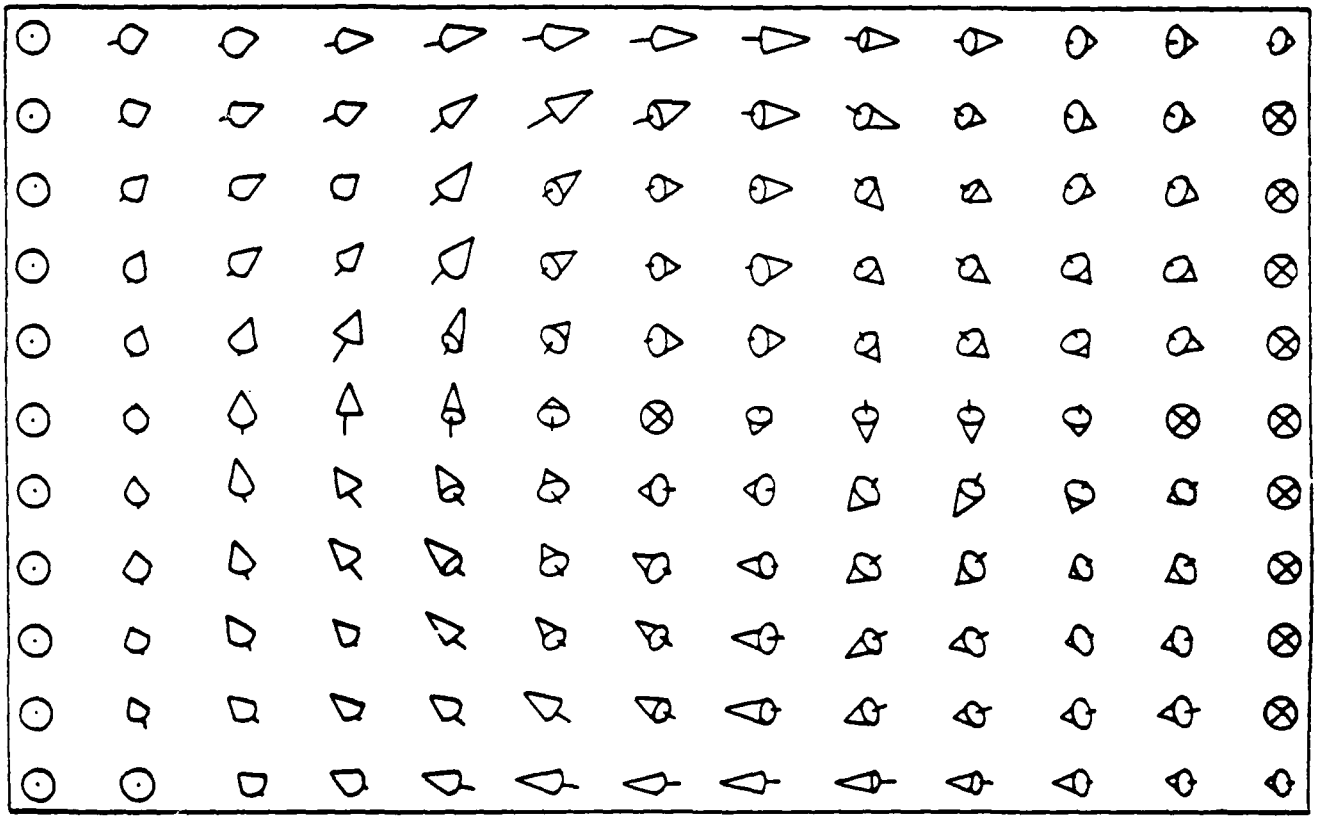

Figure 14. The magnetization in a wall region of a permalloy film 0.1 μm thick. The computation of the exact behavior of domain walls in conductors is based on the minimization of the interaction energies, including the magnetostatic energy. Of note is the fact that the magnetization always lies parallel to the surface of the conductor, thus minimizing the magnetostatic energy. Adapted from A. Aharoni[11].

END

5-81

DTIC